

# Density and lithospheric strength models of the Yellowstone–Snake River Plain volcanic system from gravity and heat flow data

Katrina R. DeNosaquo<sup>a,\*</sup>, Robert B. Smith<sup>a</sup>, Anthony R. Lowry<sup>b</sup>

<sup>a</sup> Department of Geology and Geophysics, University of Utah, Salt Lake City, UT 84112-0111, USA

<sup>b</sup> Department of Geology, Utah State University, Logan, UT 84322-4505, USA

## ARTICLE INFO

### Article history:

Received 28 May 2008

Accepted 15 August 2009

Available online 24 August 2009

### Keywords:

Gravity  
Yellowstone  
Snake River Plain  
magma  
volcanism  
rheology  
density

## ABSTRACT

The structure and composition of the Yellowstone–Snake River Plain (YSRP) volcanic system were analyzed using gravity data taken at over 30,000 stations in the YSRP and surrounding region. Additional constraints were provided by tomographic seismic velocity models, new heat flow and temperature information, GPS-derived strain rates, earthquake locations, and chemical analyses of volcanic rocks. P-wave velocity models and velocity–density data based on petrologic information were used to constrain three-dimensional density models. Rheology and strength properties were calculated at selected locations and compared to earthquake focal depths. Results of this study suggest that the lower crust of the Snake River Plain (SRP) has been thickened by the addition of an underplated layer composed primarily of clinopyroxene, having a density of 3200 kg/m<sup>3</sup>. A mid-crustal high-density sill is composed of a series of gabbroic lenses inter-fingering with the granitic upper crust. This geometry yields a bulk composition comparable to diorite and a density of 2900 kg/m<sup>3</sup>. The mid-crustal sill varies from 4 to 11 km in thickness, resulting in a series of SE–NW-trending gravity highs observed along the axis of the SRP. The mid-crustal sill extends up to 20 km southeast of the SRP volcanic field and causes asymmetry of the gravity field. The Yellowstone Plateau volcanic field density model reveals low-density partial melt 10 km beneath the caldera that shallows under the northeastern caldera, and continues laterally 20 km north of the caldera boundary and notably increases the previously estimated size of the magma reservoir by ~20%. The caldera melt body has a density of 2520 kg/m<sup>3</sup> and a significantly lower value of 2470 kg/m<sup>3</sup> for the northeastern caldera melt body. Southwest of Yellowstone, the crustal section occupied by the mid-crustal sill in the SRP and the partial melt in Yellowstone constitute a transition area between the active Yellowstone magma system and the now volcanically quiescent SRP, with a density of 2820 kg/m<sup>3</sup>. Strength models show that the crust of the YSRP becomes progressively stronger and cooler with increasing distance from Yellowstone, and tectonic earthquakes within the Yellowstone caldera are unlikely to nucleate below 4–6 km depth, thus limiting the maximum magnitude of earthquakes to  $M \leq 6.5$ .

© 2009 Elsevier B.V. All rights reserved.

## 1. Introduction

### 1.1. Volcanic and tectonic history

The Yellowstone–Snake River Plain volcanic system (YSRP, Fig. 1) provides a unique area to observe the processes of an active continental hotspot and its interaction with a continental plate. In its 17 million year history the Yellowstone hotspot has dramatically modified the landscape from southeastern Oregon to northwestern Wyoming, destroying mountain ranges, producing a chain of bimodal basalt–rhyolite volcanic centers, and forging the world famous hydrothermal features of Yellowstone National Park. These features are the collective product of hotspot derived basaltic–rhyolitic volcanism that

has and continues to reconstruct large portions of the deep continental interior. The striking surface features of the YSRP reflect the interaction of volcanic and tectonic processes that have been widely studied but remain poorly understood.

The study area for this analysis encompasses the YSRP, the adjacent Basin and Range province to the south, the Idaho batholith to the northwest, and the Rocky Mountains to the north and east (Fig. 1). This area is geologically and tectonically diverse and provides a framework in which to study the regional effects of hotspot volcanism on continental lithosphere. We note that the volcanism of the YSRP also extends northwest into the High Lava Plains of Oregon to the Newberry caldera, but our study only considers the eastern SRP and Yellowstone components of the system. Moreover we refer the reader to detailed summaries of the geology and tectonics of the YSRP as background information for our papers (see the multiple papers in this volume and Armstrong et al., 1975; Bonnicksen, 1982; Leeman, 1982; Christiansen, 2001; Camp and Ross, 2004).

\* Corresponding author. Now at ConocoPhillips, 600 N. Dairy Ashford, Houston TX 77079-1175, USA.

E-mail address: [Katrina.R.DeNosaquo@ConocoPhillips.com](mailto:Katrina.R.DeNosaquo@ConocoPhillips.com) (K.R. DeNosaquo).

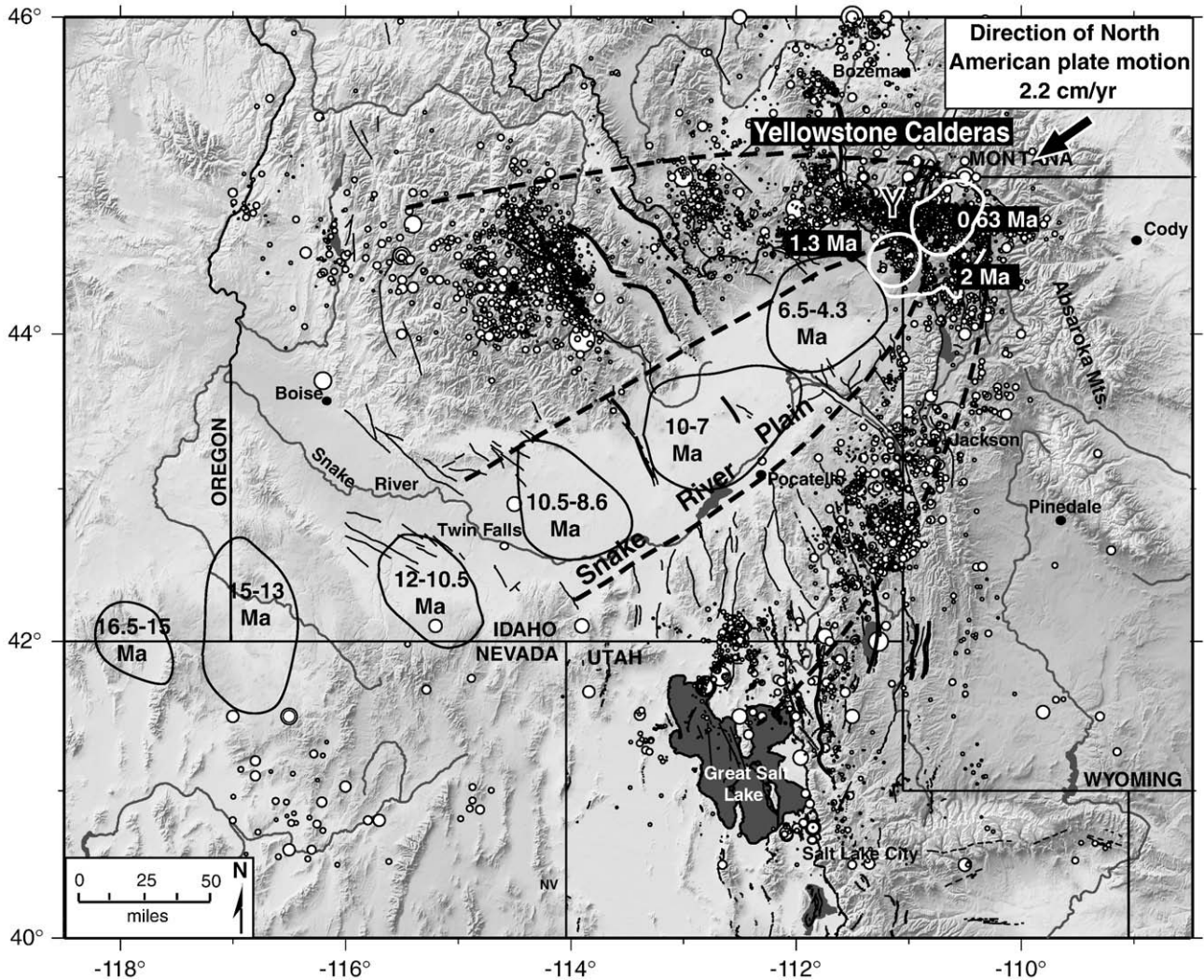


**Fig. 1.** Volcanic and tectonic features of the Yellowstone–Snake River Plain (YSRP) system. The YSRP study includes southern Idaho, western Wyoming, and southwestern Montana. Y = Yellowstone National Park. Figure after Smith and Siegel (2000), Humphreys et al. (2000), and Christiansen et al. (2002).

The YSRP volcanic system provides the record of both past and present intraplate volcanism. The time transgressive nature of YSRP volcanism was first documented by K–Ar dating of volcanic rocks in the SRP (Armstrong et al., 1975). As the North American plate has moved southwest at  $\sim 2.5$  cm/yr over the hotspot, it has left an 800 km track of giant-caldera forming volcanoes in its wake (Smith and Braile, 1993). More than  $\sim 150$  giant caldera-forming eruptions are concentrated in a dozen volcanic centers and the entire area was later covered with Late Quaternary basalt flows that form the dominant surficial features of the SRP (Perkins and Nash, 2002). Two million years ago, the Yellowstone hotspot reached its current position at Yellowstone National Park, creating the Yellowstone Plateau volcanic field as a product of plume plate interaction and three giant silicic eruptions at 2.1, 1.2, and 0.64 Ma (Christiansen, 1984). The youngest of the cataclysmic eruptions formed the modern Yellowstone caldera in Yellowstone National Park (Christiansen and Blank, 1969).

### 1.2. Regional geophysics

The varied geologic history of the study area is reflected in its geophysical signatures. A companion paper by Smith et al. (2009-this volume) provides more detail on geophysical properties of the YSRP. This paper focuses on compositional, thermal, and strength properties illustrated in gravity, seismic, and heat flow data.

Many gravity studies have been done for the YSRP, particularly in Yellowstone. Carle et al. (1990) most recently summarized the results of these surveys. Yellowstone exhibits a large negative Bouguer anomaly of about 250 Mgal. Schilly et al. (1982) resolved a mid-crustal body of low seismic velocities that corresponds to the area of the negative gravity anomaly in Yellowstone. Seismic velocity and density are generally positively correlated, thus a decrease in velocity usually corresponds to a decrease in density. The low-velocity, low-gravity area was inferred to be an area of partial melt in the upper crust.

Gravity studies of the SRP were summarized by Mabey et al. (1974) who conducted the first comprehensive study of the crustal structure using the Bouguer gravity field of southern Idaho centered on the SRP. The locally high ( $-100$  Mgal) gravity signature of the SRP can be attributed to a roughly trapezoidal mid-crustal sill-like body at the base of the upper crust (Sparlin et al., 1982). This body has a relatively high density of  $2880 \text{ kg/m}^3$ , approximately  $200 \text{ kg/m}^3$  denser than the surrounding rocks. The mid-crustal body is inferred to be mafic remnants of old magma chambers associated with the basaltic–rhyolitic volcanism of the YSRP.

Earthquakes in the study area are concentrated in a  $\sim 100$  km wide, generally north-south-trending zone of relatively shallow events and a surrounding zone north of the SRP forming an integral part of a “tectonic parabola”. The most intense seismicity is in the Yellowstone plateau and surrounding areas. Earthquakes of the YSRP dominantly

occur on normal faults and make up the central part of the Intermountain Seismic Belt (ISB) (see White et al., 2009–this volume, 2009 for a summary of the seismicity of the central ISB). However, there is variability in focal depths between different geologic provinces and thermal regimes. Seismicity is controlled by the strength of the crust, which in turn is heavily dependent on the temperature and thermal gradient. The crust does not fail by faulting below the brittle–ductile transition because rocks deform by other rheological mechanisms at much lower stress (Smith and Bruhn, 1984).

Earthquake focal depths can provide an estimate of the depth to the brittle–ductile transition. The average focal depth in the Yellowstone caldera is very shallow, often less than 4 km (Husen et al., 2004; Smith et al., 2009–this volume). This is attributed to the extremely high heat flow and temperatures that restrict brittle fracture to temperatures  $< \sim 400$  °C–500 °C. The SRP is seismically quiescent at the M3 level. The maximum focal depth in the SRP is around 8 km (Jackson et al., 1993), shallower than in surrounding provinces. This too can be explained by anomalously high heat flow, presumably resulting in a thinner brittle layer.

## 2. Gravity data and method of analysis

### 2.1. Data preparation

The data for our discussion consist of gravity observations (Fig. 2) conducted primarily by the United States Geological Survey (USGS)

and the University of Utah, and subsequently compiled by organizations including the National Image and Mapping Agency (NIMA) and the Pan American Center for Earth and Environmental Sciences (PACES, <http://paces.geo.utep.edu/research/gravmag/gravmag.shtml>). The observations were made with respect to the North American Datum of 1927 (NAD 27) and were terrain corrected using a digital elevation model developed by the USGS.

The complete Bouguer anomaly (assuming a density of 2670 kg/m<sup>3</sup>) was used in this analysis. First, the data were filtered to remove the short wavelength (basin-scale) features and the long wavelength features related to deep mantle variations. Wavelengths greater than 800 km were removed, as were wavelengths less than 40 km. The magnitude of the resulting anomaly is consistent with that used by Krukoski (2002) in an earlier gravity study of Yellowstone. The filtered data were then re-gridded with a grid spacing of 0.05°. No regional trend was removed from the data because the modeling software automatically shifted the calculated anomaly to make it comparable to the observed anomaly. The results of the filtering are shown in Fig. 3.

### 2.2. Method of analysis

The modeling method used here is summarized by Blakely (1996). Complete Bouguer gravity data were modeled using the Interactive Gravity and Magnetic Application System (IGMAS) (Schmidt and Gotze, 1998). The IGMAS algorithm calculates the three-dimensional gravity field based on an assumed 2.5-dimensional density model

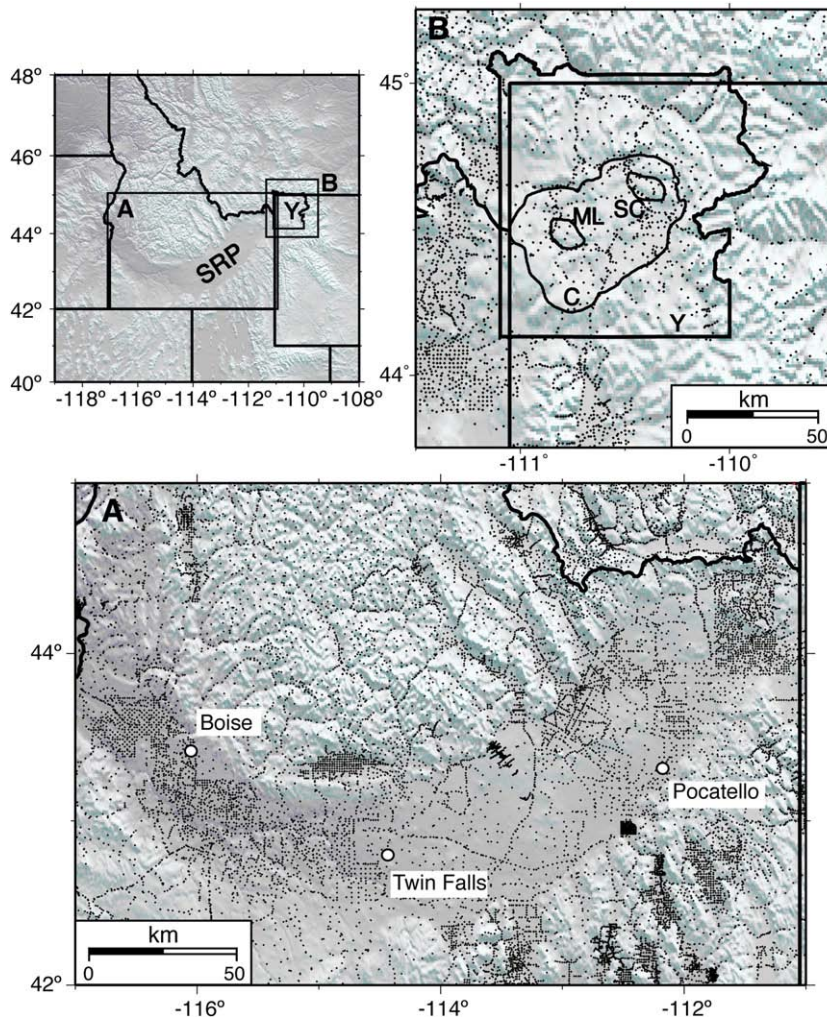
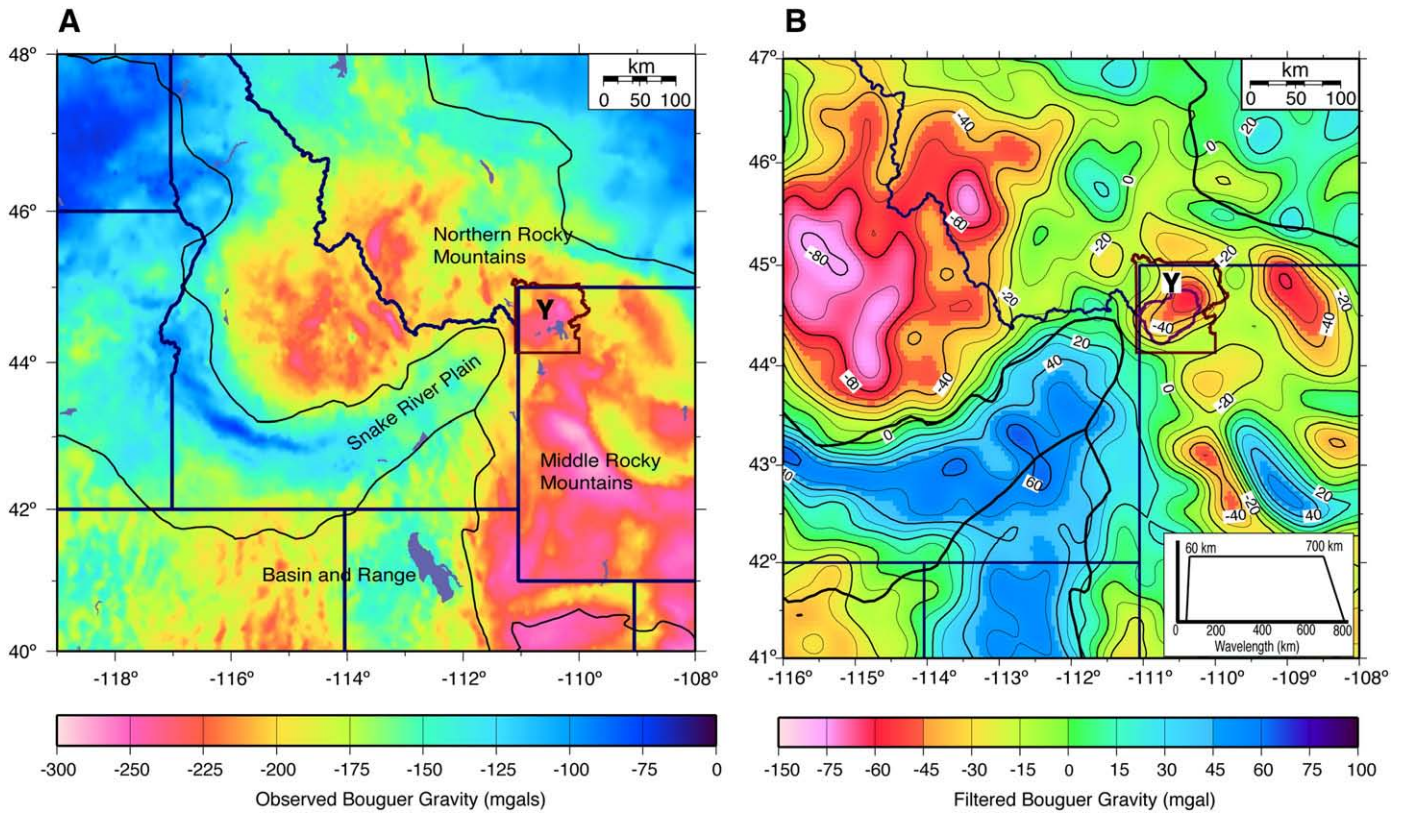


Fig. 2. Map showing the distribution of gravity stations in the SRP (A) and Yellowstone (B). Black dots are gravity stations. Yellowstone National Park (Y), the Snake River Plain (SRP), the 0.6 Ma Yellowstone caldera (C), Mallard Lake resurgent dome (ML), and Sour Creek resurgent dome (SC) are marked.



**Fig. 3.** (A) Complete Bouguer gravity anomaly map of the YSRP and surrounding area. Data provided by the online archive of the Pan American Center for Earth and Environmental Sciences (PACES). (B) Bouguer gravity anomaly map of the study area after band pass filtering for wavelengths from 40 to 800 km. Yellowstone National Park is outlined in red. Geologic province boundaries are shown with thin black lines.

built with a set of cross sections in vertical planes defined by two points on the surface and a depth. Vertical planes must always be parallel to each other, but the distance between them is variable, allowing for greater resolution in areas with more structural variability. The YSRP model has 32 vertical planes spaced 10–20 km apart plus two, planes located far outside the study area to reduce edge effects. This spacing over-samples the filtered data but produces a smooth anomaly. The origin was chosen to coincide with a density model of the SRP derived from a seismic refraction profile of the high-velocity and high-density mid-crustal sill (Sparlin et al., 1982).

### 3. Density model for the Yellowstone–Snake River Plain volcanic field

#### 3.1. The Snake River Plain density model

The starting velocity–density model for the SRP region was taken from Sparlin et al. (1982) and a seismic receiver function analysis by Peng and Humphreys (1998). Tomographic P-wave velocity models of the intermountain region by Lynch et al. (1997) and Lynch (1998) provide additional constraints. The seismic refraction studies by Braile et al. (1982) and Sparlin et al. (1982) and the receiver function analysis by Peng and Humphreys (1998) resolved two-dimensional crustal structure along approximately the same line (Fig. 4). The sill-like body these studies imaged at the base of the upper crust is also resolved in the P-wave tomographic images of Lynch et al. (1997) and Lynch (1998), as well as the surface wave analysis of Stachnik et al. (2008). The Sparlin et al. (1982) and Peng and Humphreys (1998) models differ primarily in the latter's inference of a layer of partial melt less than 5 km thick at the base of the lower crust. Peng and Humphreys also interpret thinning of the lower crust beneath the SRP.

A vertical cross section of density corresponding to the locations of the above models is shown in Fig. 5A. Densities used in the modeling were determined petrologically via a method described in Section 4. The composition of the upper crust was assumed to be granitic, the lower crust mafic granulite, and the mantle predominantly dunite, yielding densities of 2670 kg/m<sup>3</sup>, 3000 kg/m<sup>3</sup> and 3300 kg/m<sup>3</sup> respectively. Thin layers of basalt (1 km and 2900 kg/m<sup>3</sup>) and rhyolite (2 km and 2500 kg/m<sup>3</sup>) form the upper-most crust. Based on its seismic velocity the sill is presumed to have an approximately dioritic composition with a density of 2900 kg/m<sup>3</sup> (Fig. 5A).

The new density model is very similar to the seismic velocity model of Peng and Humphreys (1998) except the gravity model infers that the lower crust thickens beneath the SRP by the addition of a 3 km thick underplated layer. When molten material rises from the upper mantle, mafic cumulates that crystallize from the liquid form a zone of magmatic underplate at the base of the crust (Shervais et al., 2006). This zone is interpreted as mantle in the Peng and Humphreys model. The geometries of the bodies were iteratively adjusted in the modeling program to fit the petrologically determined densities. If the mantle density of 3300 kg/m<sup>3</sup> is used instead of the 3200 kg/m<sup>3</sup> petrologically determined density for the underplated layer (as in the Peng and Humphreys model) the density model does not fit the data.

The basal crustal underplated layer is overlain by 2 km of mafic partial melt with a density of 2850 kg/m<sup>3</sup>. The mid-crustal sill has a density of 2900 kg/m<sup>3</sup>. The upper crust thickens northwest into the NRM, while south of the SRP the crust is 2 km thinner in the Basin and Range province.

The modeled crustal structure in Fig. 5A explains the broad, incrementally decreasing gravity high that continues ~50 km beyond the southern topographic border of the SRP (Fig. 3). Why the sill extends only beyond the southern boundary of the SRP is unclear, but

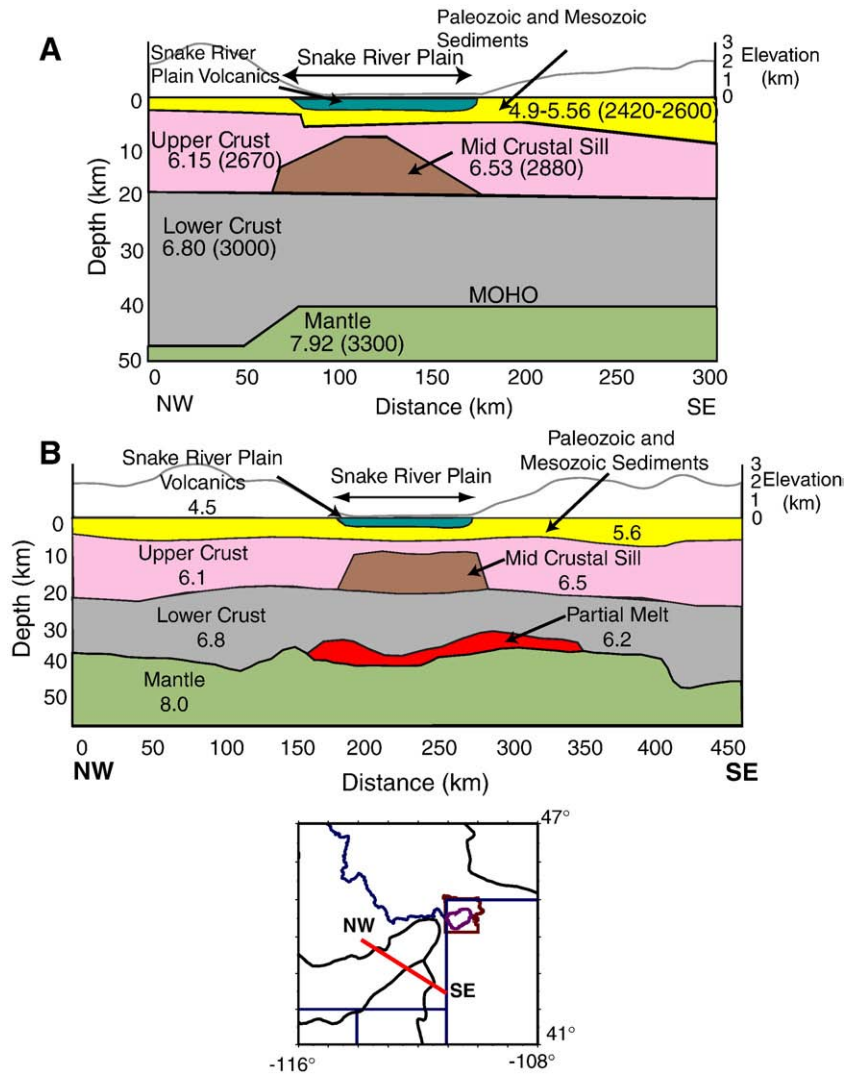


**Fig. 4.** (A) Crustal structure of the SRP determined from the seismic refraction study of Sparlin et al. (1982). (B) Crustal structure of the SRP determined from the seismic receiver function analysis of Peng and Humphreys (1998). Red line on the map represents the approximate location of both profiles. Velocities in km/s. Numbers in parentheses are densities in  $\text{kg/m}^3$ . Lines above the models represent generalized topography (km above sea level).

it may be related to a band of Tertiary normal faults and implied crustal extension that are now inactive. These faults accumulated offsets greater than 500 m coincident with caldera-forming volcanism in the SRP, and are not present on the northern side of the plain (Pierce and Morgan, 1992; Smith and Braile, 1993).

The main difference between the fault zones of Pierce and Morgan (1992) and Smith and Braile (1993) is that the latter has only three zones, including the active seismicity of the tectonic parabola, whereas the former suggested a fourth zone adjacent to the south side of the SRP that has major Tertiary faults but with little evidence of Quaternary slip and thus is an asymmetric area compared to the fault zones north of the SRP. Pierce and Morgan (1992) suggest that the distribution of faulting in their belt IV southeast of the SRP is therefore asymmetric with their belts I, II, and III on the north and south sides. In the classification of Smith and Braile (1993), faults closest to the SRP generally have low rates of seismicity compared to the area northwest of the SRP. Faults approximately 80–100 km from the boundaries of the SRP are characterized by having minimal offsets in the post-glacial period of the last 14,000 years and their driving mechanism is related to downward lithospheric flexure and downwarp into the SRP asso-

ciated with the thermal relaxation of the Yellowstone hotspot track. The active earthquake zone surrounding the SRP is more than 100 km from its boundaries. Further evidence for the asymmetric nature of SRP tectonism from Fig. 5B shows bands of seismicity extend further beyond the southern side of the plain than they do the northern side, emphasizing the asymmetry of the system. Moreover, our gravity analysis suggests that YSRP volcanic mechanisms extend well beyond the southeastern border of the plain. The presence of the sill southeast of the plain could produce asymmetrical stresses in the crust, resulting in the observed pattern of faulting. The mid-crustal sill acts as a negative isostatic load, causing the SRP to subside. Although no detailed numerical modeling was done for the area south of the SRP, our density model suggests that the strength of the bending moment of the overlying layers may reduce seismicity in zones I and II. The seismic zone immediately south of the plain also coincides with a zone of reduced seismicity, indicating that the properties of the crust south of the plain are more similar to those in the SRP than they are to those in the Basin and Range province.

The lateral extent of the SRP mid-crustal sill beyond the southern border of the SRP may also explain why in the last 5 million years,

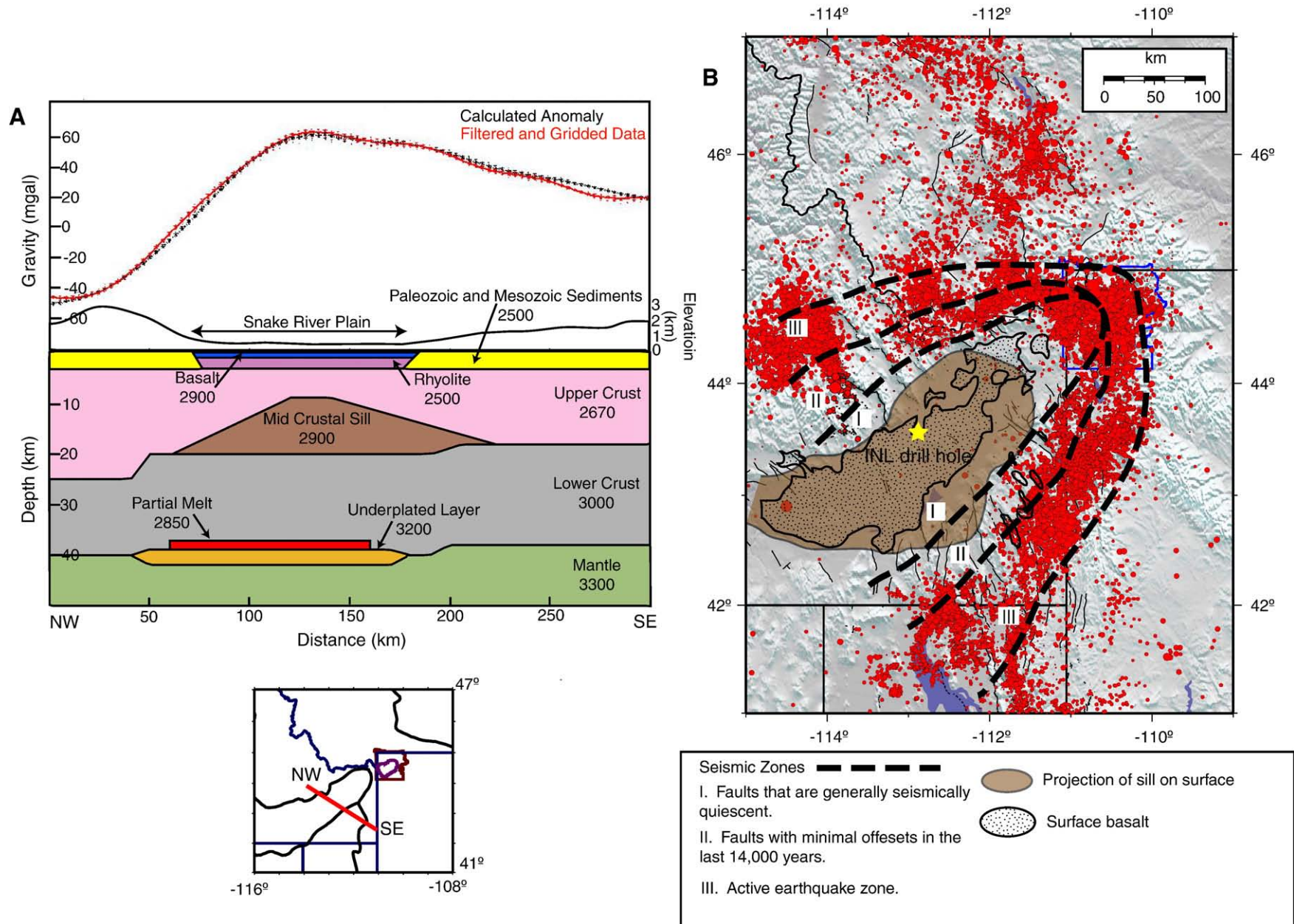


**Fig. 5.** (A) Cross-section through the YSRP density model (location indicated by the red line on the index map). This location coincides with the area of previous studies of Sparlin et al. (1982) and Peng and Humphreys (1998). All densities in  $\text{kg}/\text{m}^3$ . The gravity high south of the SRP is modeled as the continuation of the mid-crustal sill up to 20 km southeast. (B) Map showing the relationship between seismic zones defined by Smith and Braille (1993), seismicity, and the extent of the mid-crustal sill from the density model. Seismicity from a compilation of historic seismicity of the central Intermountain west by Ivan Wong (2006, personal communication) and updated for earthquake catalog data of the Montana Bureau of Mines and Geology, the Yellowstone seismic network (University of Utah Seismograph Stations, UUSS), the Idaho National Laboratory, the Jackson Lake seismic network, U.S. National Seismic Network and the Utah seismic network (UUSS).

basaltic volcanism has been more voluminous to the south of the plain than to the north. This implies that a magmatic source similar to the one beneath the SRP also exists south of the plain.

Variations in gravity along strike of the SRP imply that the sill body does not have constant thickness (Fig. 6A). There is additional evidence of this irregular geometry in the seismic P-wave tomography of Lynch et al. (1997; see also Fig. 6C). Assuming the  $V_p = 6.6$  km/s velocity zone roughly approximates the top of the mid-crustal sill, its depth varies from ~14 to ~23 km. This structure is spatially consistent with the small NW–SE-trending gravity highs within the SRP. Processes of crustal magma ascent may explain this undulating geometry. Magma may preferentially ascend through regions of the crust already thermally modified by previous magmatic intrusions or along pre-existing zones of weakness such as buried normal faults of Basin–Range extension origin and may continue to follow the established conduit until the North American plate has moved far enough that the old conduit is no longer viable (Fig. 6B). At this point, a new conduit is established and the process repeats itself, resulting in a thicker sill at the conduit locations. Density modeling is inherently nonunique, and there are other geometries that could also produce the gravity highs in the SRP. For example, the top of the lower crust could have topography, as could the bottom of the rhyolite layer. However, there is no seismic evidence for variable thickness of the lower crust, and a rhyolite layer thicker than 3 km is not geologically reasonable.

However, several lines of evidence support our new density model of the SRP, and particularly our conclusion that the SRP lower crust has experienced little or no net thinning. First, the new model fits the gravity data with only minor modifications to independent seismic imaging. The interpretation of mafic lower crustal melt feeding a felsic upper crustal magma chamber is supported petrologically (Nash et al., 2006), and by the unusually high  $\text{CO}_2$  flux at Yellowstone (Lowenstern and Hurwitz, 2008). Finally, to produce a given volume of rhyolitic melt in the upper crust, up to 10 times that amount of basalt must be intruded into the lower crust (Crisp, 1984). The history of voluminous, caldera-forming silicic eruptions associated with the Yellowstone hotspot implies an enormous amount of mafic melt intruded into the lower crust. Extension and lower crustal outflow is thought to have accommodated some of this additional mass (McQuarrie and Rodgers, 1998), but these mechanisms are unlikely to entirely erase such a large mass flux. Thus, it is possible that the lower crust in the SRP has net-thickened rather than thinned. This hypothesis is also supported by the isotope analyses of Hildreth et al. (1991), which show that Yellowstone rhyolites are derived from the melting of young, underplated mafic crust rather than felsic upper crust.

### 3.2. Yellowstone density model

The starting model for the Yellowstone volcanic field incorporates results from crust–mantle models derived from seismic refraction studies by Smith et al. (1982) and Schilly et al. (1982), three-dimensional P-wave tomographic imaging of Yellowstone by Husen et al. (2004), and the tomographic analysis of the Intermountain Seismic Belt by Lynch et al. (1997). The velocity structure of Yellowstone reveals an unusual P-wave low-velocity (4.0 to 4.8 km/s) anomaly at depths of ~3–9 km beneath the caldera that is inferred to be a zone of partial melt (Schilly et al., 1982). The more detailed and higher resolution tomography of Husen et al. (2004) indicates that the anomaly has a P-wave velocity as low as 4.6 km/s and is shallower near the Mallard Lake and Sour Creek resurgent domes.

A vertical cross section under Yellowstone is shown in Fig. 7B. Gravity modeling assumed a granitic upper crust, a mafic granulite lower crust, and a predominantly dunite mantle with densities of 2670, 3000 and 3300  $\text{kg/m}^3$  respectively. The low velocity body in this cross section corresponds to a zone of presumed partial melt with a density of 2470  $\text{kg/m}^3$ , estimated petrologically as described in

Section 4. The basal crustal underplated layer and overlying thin partial melt observed in the SRP are still present in the Yellowstone model, and have identical densities. Our density model of Yellowstone (Fig. 7B) infers variable density of the partial melt and a geometry that does not correlate exactly with tomography of Husen et al. (2004). Partial melt at ~5 km depth beneath the Mallard Lake and Sour Creek resurgent domes is not resolved in the density model, in part because of the high frequency filtering of gravity data. Our model suggests partial melt beneath the caldera at a depth of 10 km. The seismic tomography models do not have ray coverage northeast of the caldera where the gravity model suggests additional partial melt. The shallowest (7 km), lowest density (2470  $\text{kg/m}^3$ ) material extends up to ~20 km beyond the northeastern boundary of the caldera consistent with the seismic gravity model of Lehman et al. (1982) and the single body gravity inversion of Krukoski (2002). Neither of the latter studies was constrained with tomographic velocity imaging.

The large density anomaly northeast of the caldera is in the area of the Hot Springs Basin Group, the largest area of hydrothermal alteration in Yellowstone. Hot Springs Basin also has reduced seismicity that may reflect high temperatures associated with the shallow body. It is plausible that heat from the partial melt drives shallow convection in the hydrothermal system.

The temperature estimated from the geotherm controls depth to the brittle–ductile transition, and temperatures in excess of the brittle limit, >~400 °C to 500 °C, could result in a thin seismogenic layer and reduced seismicity. The reduced earthquake occurrence also limits the tomographic resolution of Husen et al. (2004), and may explain why that study did not image low velocity outside the caldera.

The hypothesized northeast caldera partial melt may also help to explain local fault distributions (Fig. 8). The Mirror Plateau Fault Zone (MPFZ) marks the northeast boundary of caldera deformation at approximately the location of the minimum gravity anomaly and the modeled partial melt. The density model (Fig. 8) infers partial melt as shallow as 7 km outside the caldera, but ~10 km within the caldera boundary. This interpretation is supported by the steeper gravity gradient of ~3 Mgal/km on the northeastern boundary of the caldera, compared to ~1 Mgal/km elsewhere in Yellowstone. Alternatively, it is also possible that the NE caldera Bouguer gravity low observed in Yellowstone may reflect features such as sediment packages underlying the edge of a Laramide thrust sheet or caldera fill after the Lava Creek eruption. However, the sharp boundary of the anomaly makes these scenarios less likely.

## 4. Velocity–density relationships

The relationship between seismic velocity and density is crucial to the joint interpretation of these complementary data types. Rather than relying on outdated velocity–density relationships to constrain the density model, a petrologic approach was applied in this study to selected rock units. Incorporation of petrologic information provides an independent constraint on our models to ensure that their geologic interpretation is reasonable. We will address the general properties of our derived density model: an underplated layer at the base of the crust, a thin layer of partial melt above the underplated layer, a sill-like mid-crustal body that characterizes the SRP, and an upper crustal partial melt body associated with the Yellowstone volcanic system.

Joint density–velocity modeling lends insight into the compositions of the mid-crustal sill and partial melt. This modeling also addresses the poorly constrained densities of partial melts that may vary by more than  $\pm 200$   $\text{kg/m}^3$  or  $\pm 10\%$  depending on the percent melt, composition, and water content. The velocity–density analysis described in this section and the density model described in the previous section were conducted iteratively, and each was adjusted based on results of the other until a final model was reached.

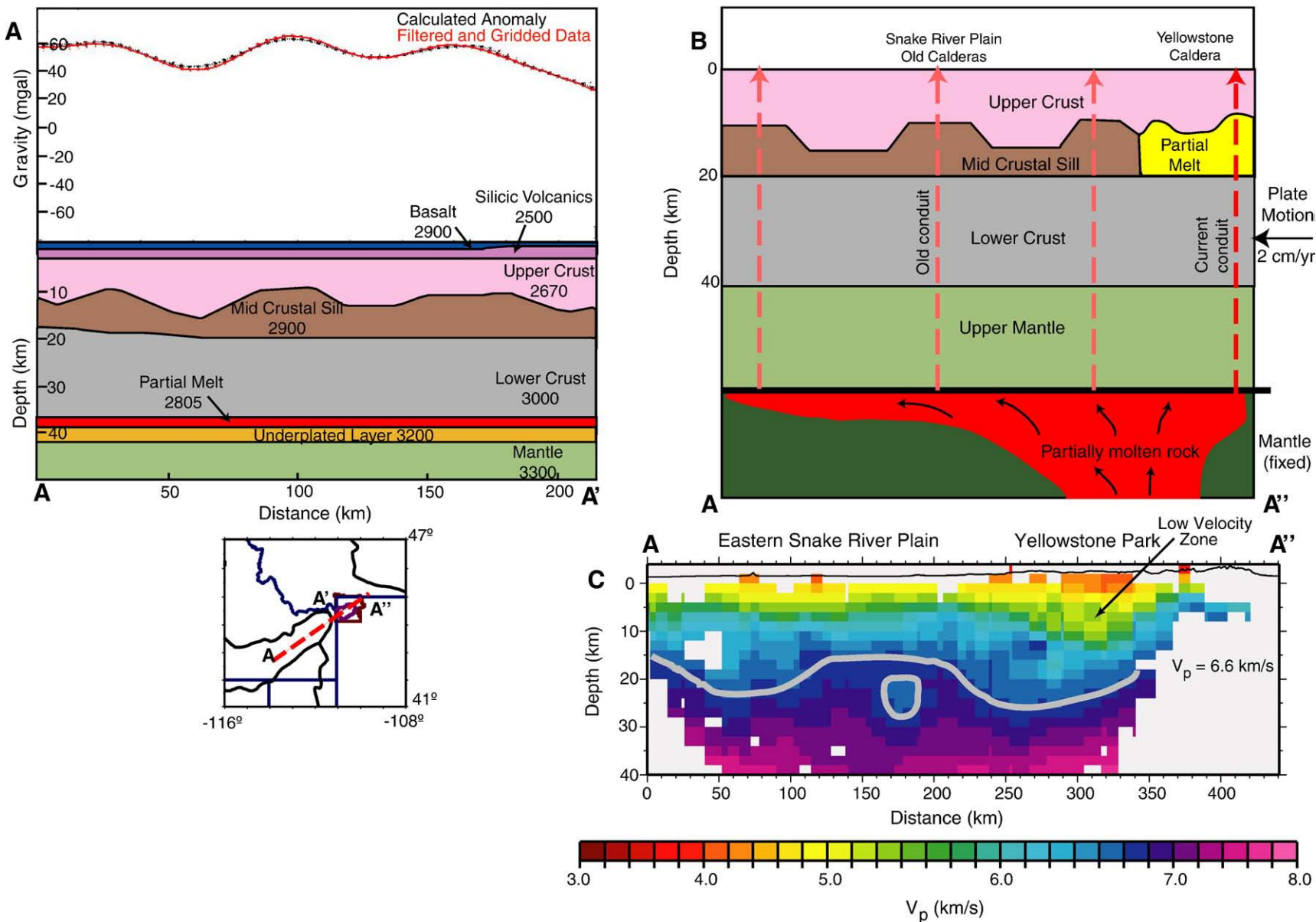


**Fig. 6.** (A) Cross-section through the density model along the axis of the SRP. A process that could produce the variable thickness observed in the mid-crustal sill is illustrated in (B) As magma rises through the crust it preferentially ascends through volumes that have already been thermally altered (indicated by red dashed lines) that serve as conduits for upwelling magma, resulting in a thicker sill at these locations. Additional support for this geometry is provided by the seismic tomographic images of Lynch et al. (1997) and Lynch (1998) (C). The  $V_p = 6.6$  km/s contour approximates the top of the mid-crustal sill, and varies in depth along the axis of the SRP.

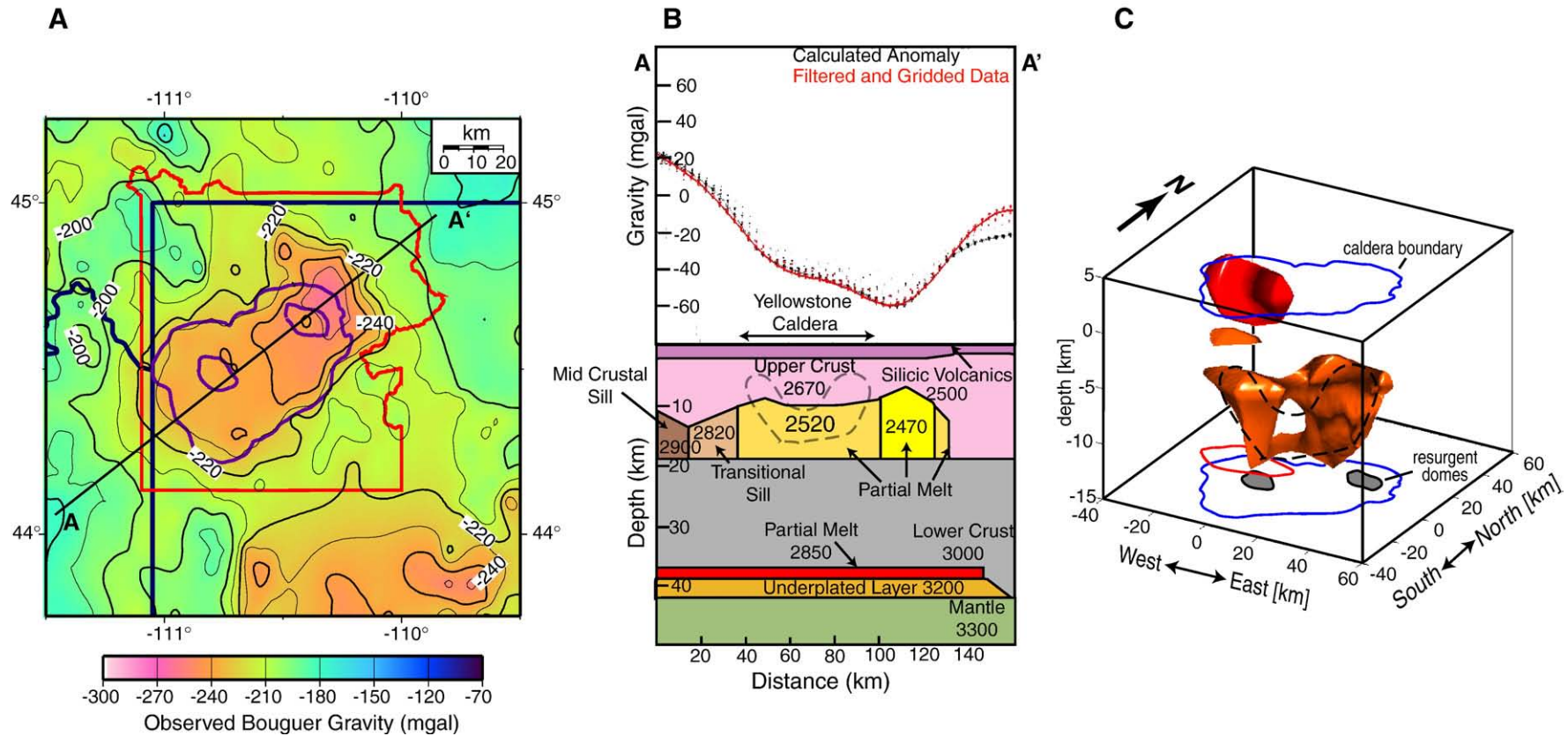


**Fig. 7.** (A) Gravity profile, and (B) Cross section through the density model for the Yellowstone area. Densities in  $\text{kg/m}^3$ . The lowest density material extends ~20 km beyond the northeastern edge of the caldera. Dashed line represents the approximate location of the seismic low velocity body tomographically imaged by Huser et al. (2004), shown in (C) The red represents a gas body inferred from  $V_p/V_s$  ratios not resolved in the density model. Mismatch between the filtered and calculated anomalies east of Yellowstone is due to basins and basement uplifts not included in the model due to their size, orientation relative to the vertical planes, and unknown properties. The steep gravity gradient in this area indicates that the body responsible for the gravity low is closer to the surface here than inside the caldera.

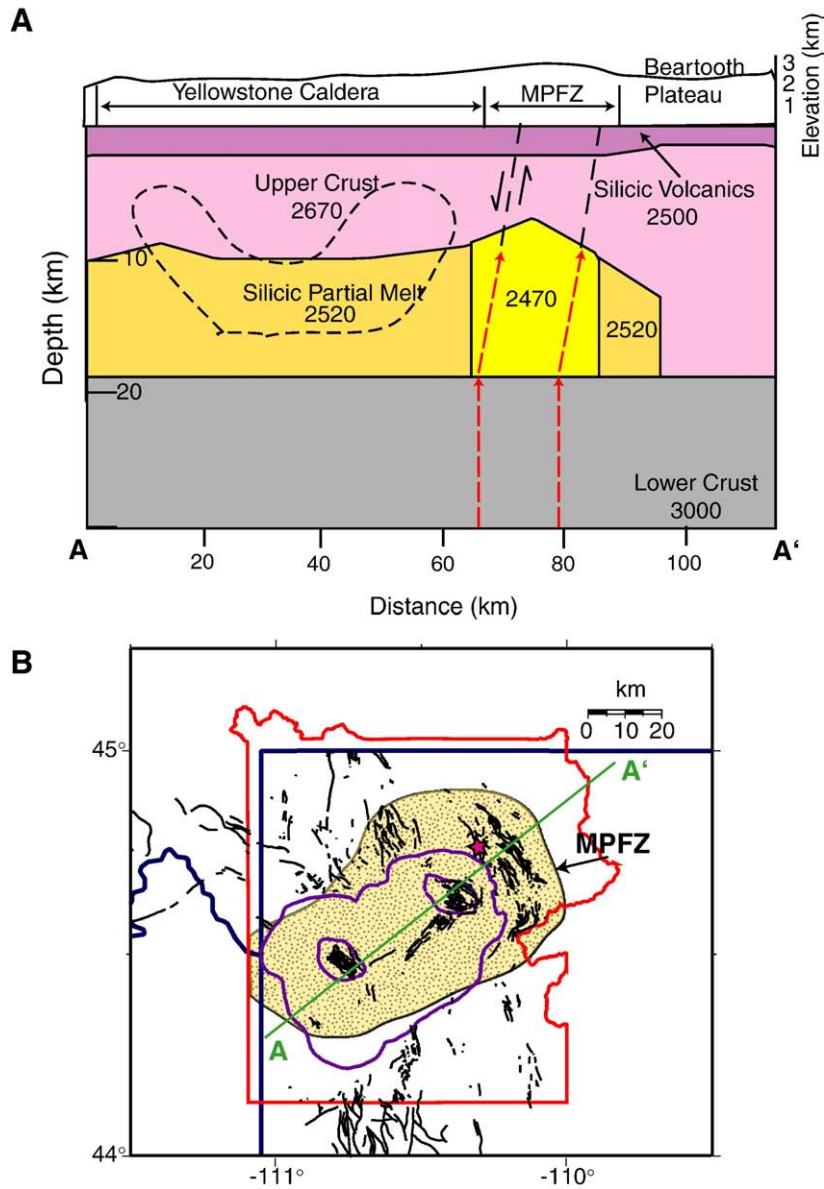


**Fig. 8.** (A) Cartoon illustrating possible magma movement northeast of the Yellowstone caldera. Southwest dipping extensional faults of the Mirror Plateau Fault Zone (MPFZ) facilitate magma movement. Densities in kg/m<sup>3</sup>. Red arrows indicate magma movement. (B) Map of the Yellowstone area. Purple outlines the 0.6 Ma caldera. Pink star is the location of Hot Springs Basin Group hydrothermal system. Yellow stipple pattern shows the lateral extent of partial melt derived from our density model.

#### 4.1. Data and method of analysis

Data for the density–velocity analysis include the results of seismic refraction studies in the YSRP and chemical analyses of volcanic rocks mapped and collected on the surface. The results of previous density studies are also used as constraints (Smith et al., 1982; Schilly et al., 1982; Braile et al., 1982; Lehman et al., 1982; Sparlin et al., 1982; Peng and Humphreys, 1998). The availability of chemical analyses limits the number of rock units that can be evaluated. It is assumed that the rock on the surface is an approximate volcanic analog to the plutonic rock at depth. The rock units in the density model that can be analyzed in this manner are the mid-crustal sill, the underplated layer at the base of the crust, and the partial melt beneath the Yellowstone caldera. Chemical analyses of primitive and average SRP basalts from Lum et al. (1989) were chosen to represent the basal crustal underplated layer and the mid-crustal sill, respectively. The composition of the partial melt beneath the Yellowstone caldera was assumed to be

similar to that of the Lava Creek Tuff deposited during the most recent caldera forming eruption 640,000 years ago.

Sparlin et al. (1982) used a detailed seismic refraction profile perpendicular to the SRP to model the velocity structure for the eastern SRP, whereas Peng and Humphreys (1998) describe a similar velocity structure based on the results of a receiver function analysis. Both studies infer a 6.5 km/s velocity for the mid-crustal sill, which is unusually high for typical Basin and Range mid crust. Sparlin et al. (1982) inferred a density of 2880 kg/m<sup>3</sup>. There is little direct seismic evidence for an underplated layer at the base of the crust, so there is no velocity data to use in the analysis, or density data to use as a constraint. However, because it is not imaged seismically, the velocity and density of the underplated layer must be similar to those of the mantle. The tomographic models of Husen et al. (2004) suggest that the Yellowstone partial melt has a velocity as low as 4.6 km/s. Krukowski (2002) assigned a minimum density of 2300 kg/m<sup>3</sup> to the partial melt based on density inversion and the density model of Lehman et al. (1982).

**Table 1**  
Crustal velocities.

	Underplated basal crustal layer		Mid-crustal sill			Yellowstone mid-crustal partial melt	
	Previous Studies	Primitive SRP basalt <sup>a</sup>	Previous studies <sup>b</sup>	Average SRP basalt <sup>a</sup>	Diorite <sup>c</sup>	Previous studies	Lava creek tuff <sup>d</sup>
Density (kg/m <sup>3</sup> )	None	3220	2880	3050	2920	2300 <sup>e</sup>	2550 <sup>f</sup>
Vp (km/s)	None	7.25	6.53	6.79	6.61	4.6 <sup>h</sup>	6.0 <sup>i</sup>

<sup>a</sup> Lum et al. (1989).

<sup>b</sup> Sparlin et al. (1982).

<sup>c</sup> Raymond (2002).

<sup>d</sup> Christensen (2001).

<sup>e</sup> Krukoski (2002).

<sup>f</sup> 10% melt assuming 0% water content.

<sup>h</sup> Husen et al. (2004).

<sup>i</sup> Melt not included in calculation.

The chemical compositions of volcanic rocks were assumed to approximate the whole rock compositions of plutonic rocks in the YSRP and included the basal crustal underplated layer, the mafic partial melt above the underplated layer, the mid-crustal sill, and the Yellowstone partial melt. The compositions of average and primitive SRP basalts and a representative Yellowstone rhyolite were evaluated using the algorithm MELTS (Asimow and Ghiorso, 1998). MELTS is an algorithm designed to model the phase equilibria of igneous systems at various temperatures and pressures. In this case, it was used to predict the mineralogical compositions of plutonic rocks crystallized from magmas having the chemical compositions described above. In the case of the basal crustal underplated layer, the algorithm pMELTS was used. pMELTS is a variation of MELTS that is optimized for mantle conditions (Ghiorso et al., 2002).

These analytical modeling codes were used to calculate the liquidus for each composition, and temperature was set to decrease in increments of 20 °C from the liquidus to the solidus. In the case of primitive SRP basalt, the basal crustal underplated layer was assumed to consist of only the first minerals to crystallize from the liquid. The Yellowstone partial melt was assumed to be the source of the youngest giant eruptive rhyolite, the Lava Creek Tuff, at approximately 10% liquid. The pressure was calculated from the depth of the rock unit and was not allowed to vary. The depth of the mid-crustal sill and the Yellowstone partial melt was set to 10 km with an equivalent stress of 300 MPa. For the underplated layer the depth was set to 40 km with a pressure of 1050 MPa.

The MELTS algorithm determines the weight percents of all minerals present at each temperature increment and predicts the density of the liquid and solid portions, and of the entire system. Weight percents of the major minerals were converted to volume percents for use in the velocity–composition algorithm of Hacker and Abers (2004). To simplify this process, all solid solutions were represented only by their end members. The Hacker and Abers method employs as input the volume percent of minerals in a rock, and the pressure and temperature of the rock. Water content, density, compressional velocity, shear velocity, bulk modulus, shear modulus, and Poisson's ratio are all generated as output but this analysis used only the density and compressional velocity. Density values for the underplated layer and mid-crustal sill were rounded to the nearest 50 kg/m<sup>3</sup>.

#### 4.2. Results and interpretation

Our crustal velocity determinations are summarized in Table 1 and illustrated in Fig. 9. The underplated layer is composed entirely of clinopyroxene with a density of 3220 kg/m<sup>3</sup> and a compressional velocity of 7.25 km/s. Though there are no previously determined velocity or density values for this layer, they must be similar to those in the mantle. A pyroxenite composition is supported by cumulate xenoliths rich in pyroxenes that have been reported in lavas west of Island Park (Leeman et al., 1985). Sparlin et al. (1982) inferred the density of the mantle to be 3300 kg/m<sup>3</sup> based on a compressional

velocity of 7.92 km/s. Significantly, the small velocity ( $\pm 0.65$  km/s) and density ( $\pm 80$  kg/m<sup>3</sup>) contrasts predicted by this analysis may not yield sufficient impedance contrasts to generate a perceptible receiver function signal. MELTS also predicts the density of the remaining liquid to be 2850 kg/m<sup>3</sup>. The high density partly reflects a pressure dependence of basaltic melt density analogous to the basalt–eclogite transition in the solid phase (Fujii and Kushiro, 1977). The average SRP basalt composition suggests that the composition of the mid-crustal sill is gabbroic, which would predict a density of 3050 kg/m<sup>3</sup> and a velocity of 6.79 km/s. The predicted compressional velocity is notably higher than observed by Sparlin et al. (1982) and Peng and Humphreys (1998), indicating that the bulk composition of the mid-crustal sill is probably not a pure gabbro. The large predicted density difference also argues against a gabbroic composition. There are no intermediate composition volcanic rocks in the YSRP, so a chemical analysis of a diorite was taken from Raymond (2002) to compare the velocity and density of the mid-crustal sill to the velocity and density of an intermediate rock. Results from MELTS and the crustal velocity and density calculations show that the density of the diorite is 2920 kg/m<sup>3</sup> and the velocity is 6.61 km/s. These values are more comparable to those observed seismically, implying that the sill has an intermediate composition consistent with a mix of gabbroic intrusives and pre-existing country rock. This result is consistent with conceptualizing the sill as composed of many small, layered mafic lenses that inter-finger with the upper crust, as described by Shervais et al. (2006). Seismic waves average the granitic upper crust and the

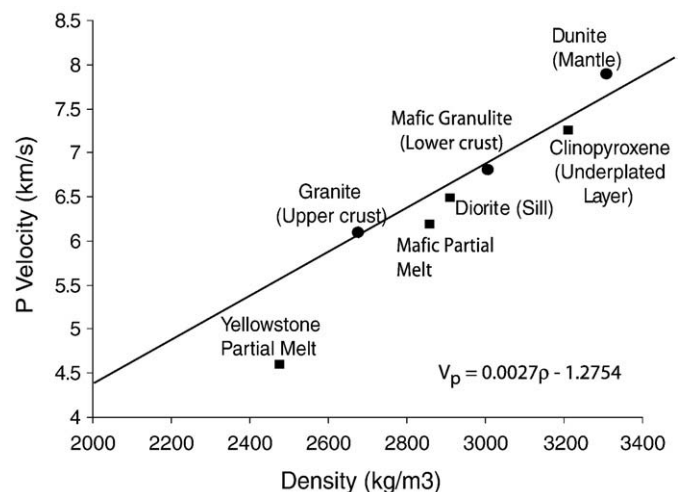


**Fig. 9.** Velocity–density plot for rocks in the YSRP volcanic field. Circles are rocks with densities inferred from other studies and squares are densities of rocks evaluated in this study. The Yellowstone upper crustal partial melt and mafic melt were not included in the calculation of the linear equation.

gabbroic lenses, imaging a single body that appears to be of intermediate composition based on its seismic velocity.

The sensitivity of density and velocity of the diorite composition to input mineral composition was analyzed by varying the volume percentages of albite, anorthite, and enstatite by  $\pm 25\%$ . These are the three most abundant minerals in the diorite composition, and together comprise about 80% of the rock. Varying the mineral composition resulted in a density variation of  $\pm 30 \text{ kg/m}^3$  and a velocity variation of  $\pm 0.12 \text{ km/s}$ . Density variations less than  $50 \text{ kg/m}^3$  are not resolvable in the density model, so the uncertainty in the density calculation is within the accuracy of the model.

MELTS was designed for basalts and other mafic compositions, and its applicability to silicic compositions like the Lava Creek Tuff is limited. Phase equilibria for felsic minerals are not well modeled by the MELTS package, so modeling of silica rich systems is hampered by methodological limitations. MELTS converged on a solution only if the water content was assumed to be zero. While the water content of partial melt beneath the Yellowstone caldera is poorly known, it is believed to be  $\sim 2\%$  ( $\pm 1\%$ ). The density and velocity of wet melts are lower than those for dry melts. Neglecting the water content in the calculation introduces errors, and the calculated density and compressional velocity will likely be greater than those in the real Earth. The calculations are further limited by the crustal density and velocity calculation, which deals only with solid rocks, and does not model melt processes. The density of the system from MELTS was taken to be the average density of the Yellowstone partial melt in Table 1. The velocity in Table 1 reflects only the solid portion of the system, and is certainly lower in the real Earth. For this reason, the calculation of  $2550 \text{ kg/m}^3$  was not used directly in the density model. Instead, it was used as an upper bound and the density was varied from the upper crustal density of  $2670 \text{ kg/m}^3$  in increments of  $50 \text{ kg/m}^3$  as in the model of Krukoski (2002). The partial melt modeled in Section 3 has densities of  $2520$  and  $2470 \text{ kg/m}^3$ , representing density contrasts of  $-150$  and  $-200 \text{ kg/m}^3$ , respectively.

## 5. Rheology and lithospheric strength

Strength modeling of the YSRP crust was conducted to assess how rheological properties relate to magmatic and tectonic processes. Here we examine the relationships of the brittle and ductile components of strength to properties such as temperature, composition, and the effective elastic thickness, and we examine whether strength modeling affords insights into why the SRP is seismically quiescent.

The thermal state of the YSRP is reflected in measurements of the regional conductive heat flow compiled for the Geothermal Map of North America (Blackwell and Richards, 2004). Deep measurements made beneath the hydrologically perturbed basalts indicate that the SRP has high ( $> 100 \text{ mW/m}^2$ ) heat flow, exceeding that in the nearby Basin and Range ( $\sim 90 \text{ mW/m}^2$ ) and Rocky Mountain ( $\sim 50 \text{ mW/m}^2$ ) provinces. SRP heat flow also increases from west to east. In the Yellowstone caldera, heat flow exceeds  $200 \text{ mW/m}^2$  and direct measurements average  $2000 \text{ mW/m}^2$ . This value is 20–30 times higher than the continental average. Also see Smith et al. (2009–this volume) for a discussion of heat flow of the Yellowstone caldera and its effect on earthquakes.

Predominantly convective heat flow in active hydrothermal areas exceeds  $20,000 \text{ mW/m}^2$  (Morgan et al., 1977). The convective contribution that dominates the signal is not readily interpretable with analytic thermal models. Nonetheless, high temperatures drive thermal buoyancy (which affects the topography) and influence the strength of the crust, thus affecting the distribution of earthquakes.

The seismic quiescence of the SRP is problematic given the evidence for late Quaternary extensional strain associated with dike intrusion. Brott et al. (1981) proposed that the SRP is seismically quiescent because crustal temperatures in the wake of the hotspot are high compared to the surrounding Basin and Range and Rocky

Mountain areas, and the heat weakens the crust, making it too weak to fail by faulting. Anders and Sleep (1992) developed a thermal–mechanical model that predicts very rapid extension due to mafic intrusions concurrent with hotspot volcanism and a subsequent lack of seismicity as the strain rate returns to its pre-hotspot value. GPS data (Puskas et al., 2007) suggest that the SRP nearest Yellowstone is experiencing limited compression between the rapidly extending Yellowstone plateau and Basin and Range blocks, and that the SRP may behave as a lithospheric block being pushed southwest with little internal deformation. Parsons et al. (1998) argue that dike intrusion of the SRP maintains the same strain rate as on the adjacent areas of active normal faulting outside the SRP with a corresponding aseismic deformation of the SRP.

New GPS observations by Payne et al. (2008) and Puskas and Smith (2009) show that the SRP is moving southwest at  $\sim 2.2 \text{ mm/yr}$  relative to  $\sim 3 \text{ mm/yr}$  at Yellowstone, implying that the SRP block may be in compression and behaving as a uniform block moving southwest from Yellowstone. Modern GPS observations indicating compression coupled with geologic evidence of Quaternary extension implies that crustal deformation is time dependent and varies under viscoelastic conditions. The new model of contemporary deformation argues that the seismic quiescence of the SRP is related to its increased strength and lack of large deviatoric stresses that would drive seismicity.

### 5.1. Heat flow and earthquake data

Data for this portion of the analysis are measurements of surface heat flow and accurately determined earthquake focal depths. Surface heat flow data were acquired from borehole temperature measurements compiled by Blackwell and Richards (2004). The heat flow data from this study were extrapolated to temperature at depth by Blackwell et al. (2007). The earthquake focal depths were compiled from earthquake catalogues between the mid 1970s and 2004 from a compilation of historic seismicity of the central Intermountain west by Ivan Wong (2006, personal communication) and updated for earthquake catalog data of the Montana Bureau of Mines and Geology, the Yellowstone seismic network, the Idaho National Laboratory, the Jackson Lake seismic network, U.S. National Seismic Network, and the University of Utah seismic network (UUS). Husen et al. (2004) relocated events that occurred in the Yellowstone network between 1995 and 2001 by simultaneously inverting for hypocenter locations and three-dimensional velocity structure. White et al. (2009–this volume) did a similar analysis of the Teton area. Jackson et al. (1993) compiled a catalog of earthquakes that were recorded on the Idaho National Laboratory network between 1973 and 1992 and showed that infrequent, small magnitude ( $M_c$  usually less than 1.5) earthquakes with focal depths less than or equal to 8 km are characteristic of the eastern SRP.

The 80th percentile of the maximum focal depths was calculated for the most accurate depths from the above data to infer the depth to the brittle–ductile transition. The 80th percentile depth has been shown by Smith and Bruhn (1984) to be the best indicator of the depth of the brittle–ductile transition for areas of extension, and thus the tectonic regime of the YSRP. In Yellowstone the focal depths are markedly shallow (with most focal depth less than 6 km beneath the center of the caldera). The SRP and surrounding area of the YSRP tectonic parabola (Smith and Braile, 1993; Smith et al., 2009–this volume) contain focal depths ranging from approximately 5 to 10 km. This is consistent with the focal depth studies of Jackson et al. (1993) that showed the maximum focal depth in the eastern SRP to be about 8 km.

### 5.2. Strength modeling

Strength profiles were produced for 5 distinct thermal regimes (Fig. 10) in the YSRP and surrounding area, including stable North America (1), the Basin and Range (2), the eastern SRP (3), the Yellowstone Plateau (4), and the Yellowstone caldera (5). The calculations

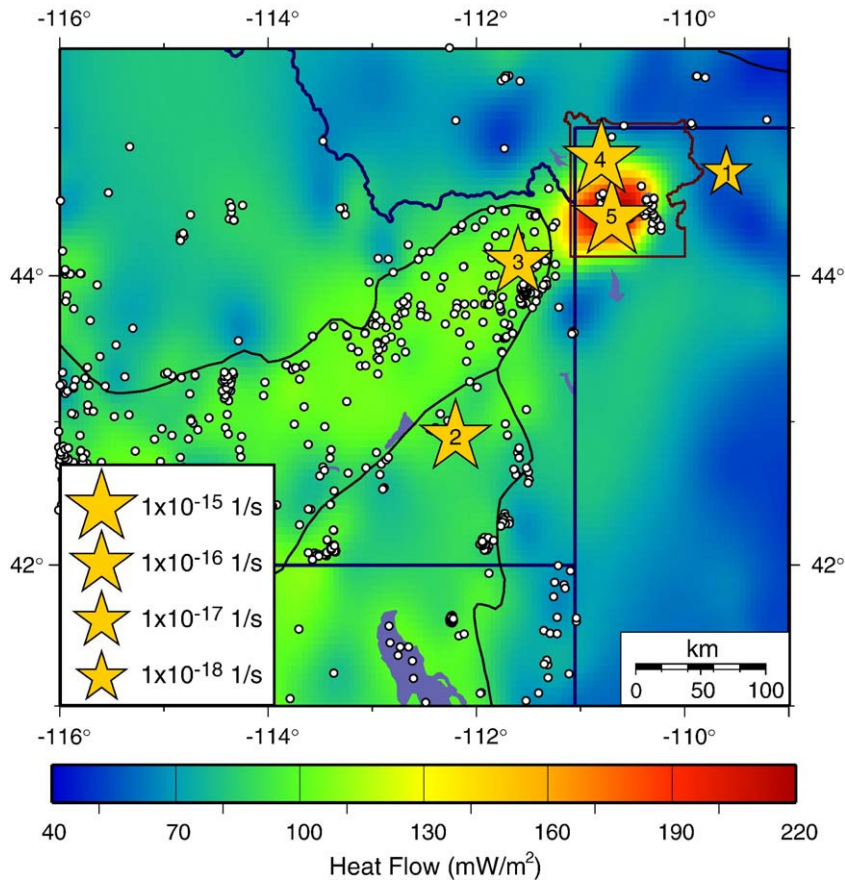


**Fig. 10.** Map showing heat flow from Blackwell et al. (2007) and the locations of the calculated strength profiles from rheologic modeling. Strain rates at each location from Puskas et al. (2007). Circles represent the location of boreholes used to determine heat flow values.

were done with the power law rheological model summarized by Smith and Bruhn (1984). Thermal gradient, rock type, stress regime, strain rate, and density are used to determine shear stress vs. depth. The model is based on the equations for brittle and ductile deformation. Brittle deformation is described by Byerlee's Law:

$$\tau = \mu\sigma_n \quad (1)$$

where  $\tau$  is the shear stress,  $\mu$  is the internal coefficient of friction (taken here to be 0.8), and  $\sigma_n$  is the effective normal stress on a fault. Ductile deformation is governed by power law creep:

$$\varepsilon = A(\sigma_1 - \sigma_3)^n \exp(-Q/RT) \quad (2)$$

where  $\varepsilon$  is the strain rate,  $R$  is the gas constant,  $T$  is temperature and  $A$ ,  $n$ , and  $Q$  represent material properties of the rock.

Temperature estimates to 10 km depth from Blackwell et al. (2007) were used to create thermal profiles at the locations shown in Fig. 10. At 20, 30, 40, and 50 km the temperature was estimated by the method described by Chapman (1986). These points were fit to a second order polynomial regression and the resulting equation was used to define the temperature profiles in the strength models. The second order polynomial fits the data points in every case except the Yellowstone caldera, where the temperatures are greater and the curve is steeper. In this case a fourth order polynomial was used to define the geothermal gradient.

Information about the material properties of rocks is often sparse and not well constrained. Eight igneous rock types are built into the model, and the composition of the crust can be represented only by these approximations. The compositions were chosen from those

available to best represent the upper and lower crust and mantle. The upper crust was assumed to be composed of dry granite, the lower crust was assumed to be diabase, and the mantle was assumed to be dunite. These rocks were chosen because their velocities and densities are similar to velocities observed in seismic studies and the densities modeled in Sections 3 and 4. Quartz diorite was chosen to represent the sill based on the results of the velocity–density analysis described in Section 4. The strain rates for each area were determined from GPS observations (Puskas et al., 2007). Strain rates vary from  $\sim 1 \times 10^{-18}/s$  in stable North America to  $\sim 5 \times 10^{-15}/s$  in the Yellowstone caldera. The thicknesses and densities of layers are taken from the density model described in Section 3. The stress regime was assumed to be extensional.

Input data and assumptions in the strength models may contribute to variations in the shear stress. For example, heat flow measurements are notoriously noisy and, when used as a proxy for deep conductive geotherm, can have uncertainties as large as 50% (Lowry et al., 2000). Heat flow and a number of estimated parameters are used to calculate the temperature at depth (Blackwell et al., 2007), thus errors in the temperature information have the potential to be as large or larger than those in the heat flow information. Typical uncertainties in GPS determined strain rates for the YSRP are on the order of  $\pm 0.03 \mu\text{e}/\text{yr}$  (Puskas et al., 2007), but surface rates may not be representative of rates for flow at depth.

Tests were performed by independently varying the thermal gradient, rock type, and strain rate to determine the sensitivity of the model to these parameters. Of all the parameters tested, thermal gradient has the greatest effect on strength. Increasing the thermal gradient can significantly weaken the crust. The effects of rock type and strain rate are secondary.

5.3. Strength models

Fig. 11 shows the results of the strength modeling at locations 3, 4, and 5, which correspond to the eastern SRP, the Yellowstone Plateau, and the Yellowstone caldera, respectively. These locations represent the track of the Yellowstone hotspot, the area immediately adjacent to the active volcanic system, and the active volcanic system itself. In the eastern SRP the brittle–ductile transition for granite occurs at about 8 km. The SRP mid-crustal sill is brittle to about 16 km depth, and the lower crust is entirely ductile. The brittle–ductile transition in the lower crust occurs at about 21 km and the mantle is entirely ductile. In the Yellowstone plateau the brittle–ductile transition occurs at about 11 km. A brittle–ductile transition occurs in the lower crust at about 27 km. The upper mantle is also brittle. Inside the Yellowstone caldera the brittle–ductile transition occurs at about 4 km (see detailed analysis by Smith et al., 2009-this volume). The lower crust and upper mantle are both ductile.

The strength profiles are influenced by limitations in our knowledge of model parameters. In this study, the brittle–ductile transition is inferred to be the point at which Byerlee's law intersects the ductile deformation curve. Water content can influence the strength of a material, but its effects are poorly known for the compositions used in this analysis. Advection in the SRP aquifer can also influence the heat flow determinations and therefore the thermal gradient, though Blackwell et al. (2007) argue that their averaged heat flow properties are reliable for this area. In the Yellowstone caldera, where the shallow hydrothermal system has a strong influence on the thermal gradient, the measured heat flow is assumed to be the conductive component but the effects of convection in these systems are not known. However, the relatively uniform thermal flux in Fig. 10 suggests that the average value used here is a good estimate of the temperature.

Despite the uncertainties in the models it is possible to draw some broad conclusions about the rheological properties of the crust in the YSRP. The crust is notably weak in the Yellowstone caldera, restricting the brittle zone to very shallow depths of ~4 km and thus limiting the maximum magnitude of earthquake nucleation to ~M6.5. The upper crustal strength increases with increasing volcanic age of the SRP, revealing a thicker and cooler upper crust. Outside the YSRP the brittle–ductile transition deepens to ~15 km or more, indicating the potential for deeper earthquake nucleation and thus for larger earthquakes.

6. Discussion

This study integrates gravity, seismic, thermal, and petrologic data to investigate the density, strength, and composition of the crust in the YSRP volcanic system. Synthesizing these results provides new insight into the structure and composition of the lithosphere and the nature of hotspot processes, including the unique properties of YSRP volcanism and tectonics.

6.1. Yellowstone volcanic field

A cross section summarizing our model of the composition and velocity–density structure of the YSRP is shown in Fig. 12. At Yellowstone, the model reflects processes of magma ascent from a mantle plume partial melt at ~1500 °C to the surface. The magma is interpreted to rise through a plexus of vertical conduits less than ~5 km in diameter, as they are not imaged in seismic tomography. One to two percent partial melt from the plume source (Smith et al., 2009-this volume) rises buoyantly from the upper mantle to a level of neutral buoyancy in the mid-crust.

YSRP basalts typically contain very little clinopyroxene (Hildreth et al., 1991), implying that they have been removed by some process prior to eruption. We propose here that when mafic melt encounters the cooler lower crust, clinopyroxenes crystallize from the melt, forming an underplated layer at the base of the crust. These cumulates have a modeled density of 3200 kg/m<sup>3</sup>. Further evidence for a clinopyroxene underplated layer comes from pyroxenite-rich cumulate xenoliths reported in lavas just west of Island Park (Leeman et al., 1985). This suggests that our hypothesis is testable by determining the depth of cumulate formation. The hypothesized underplated layer would thicken the lower crust, partially offsetting flow-related thinning in response to the mid-crustal load.

After pooling atop the underplated layer long enough to shed dense cumulate minerals, the remaining liquid ascends buoyantly, assimilating wall rock in the conduit along the way. The rarity of mantle xenoliths suggests a slow rate of magma ascent and long residence times in the crust. Thus, it is likely that significant crustal assimilation could occur (Hildreth et al., 1991). The amount of crustal assimilation at a particular location probably decreases with time as conduits of processed crust are established (Shervais et al., 2006). Snake River Plain basalts are commonly characterized as theoleiitic,

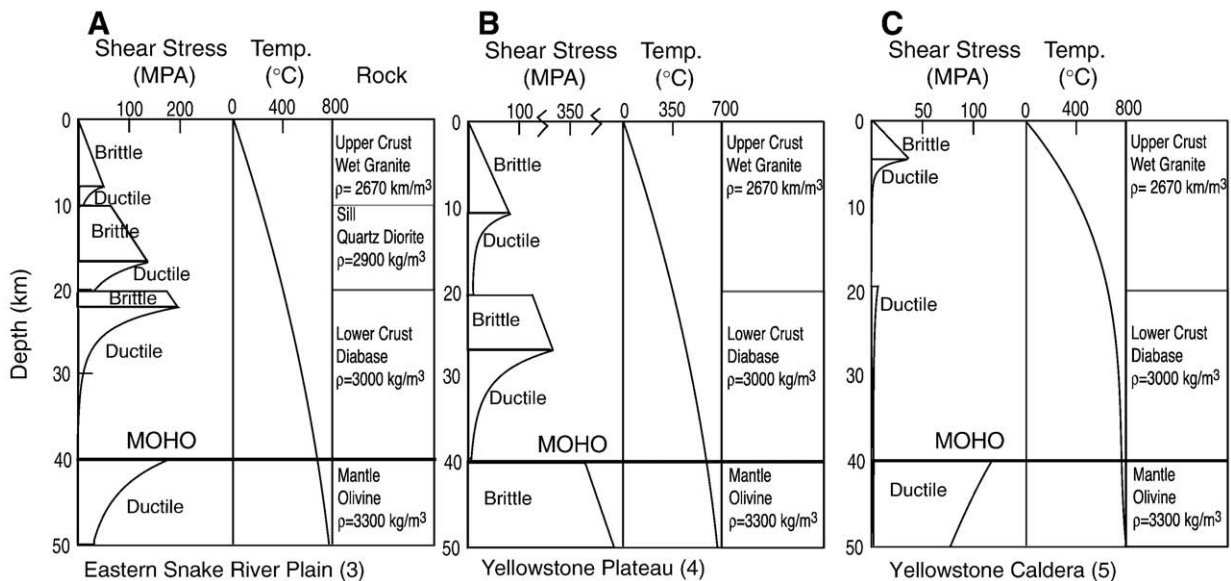
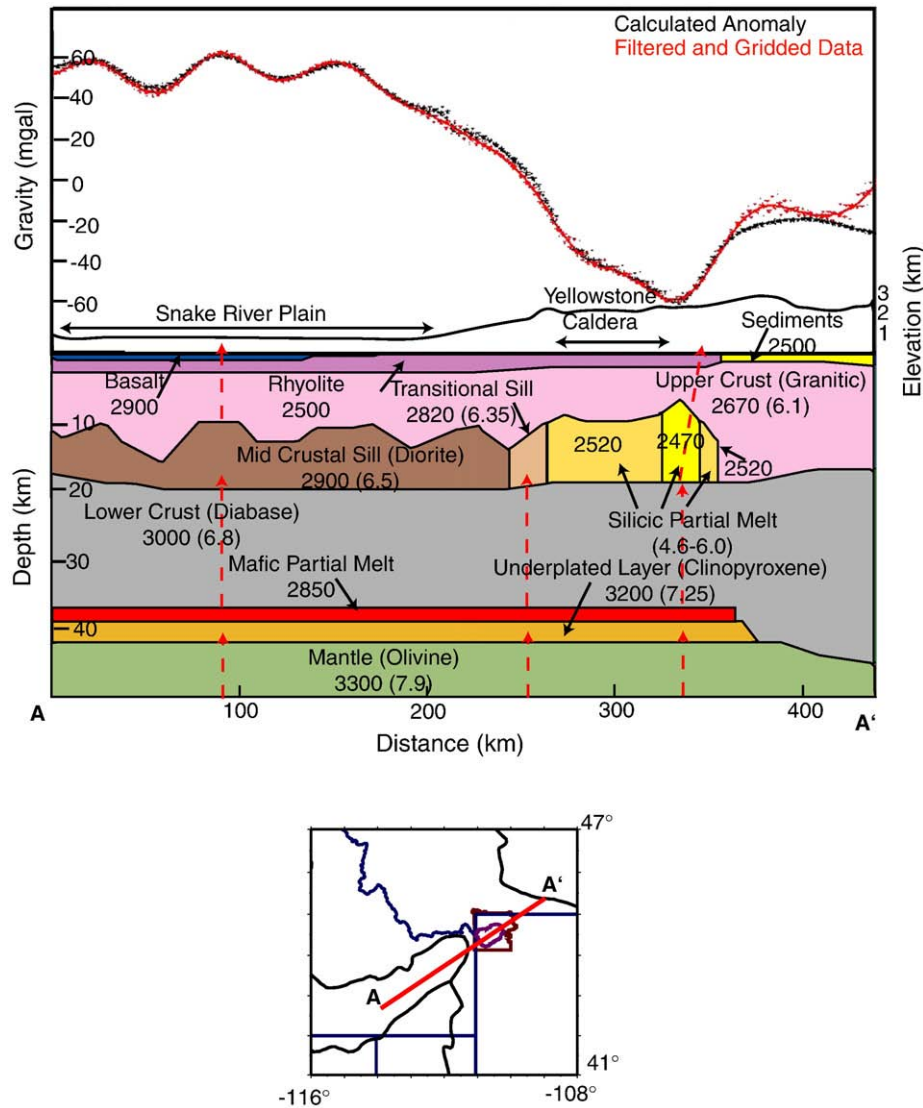


Fig. 11. Strength models of the eastern SRP, Yellowstone Plateau, and Yellowstone caldera. Profile locations and respective strain rates are shown in Fig. 10.



**Fig. 12.** Cross section of the YSRP density model reflecting the results of previous studies and the velocity–density composition analysis of this study. Numbers in parentheses represent P wave velocities (km/s). Line above cross section represents the generalized topography (km above sea level).

and primitive, uncontaminated lavas are uncommon. Large-volume Yellowstone ignimbrites and smaller volume post-caldera lavas require remelting of large volumes of  $^{18}\text{O}$ -depleted volcanic rocks altered by hydrothermal activity (Bindeman et al., 2008). The geochemistry suggests that each post-caldera lava represents an independent homogenized bath of magma that was generated rapidly by remelting of source rocks. The conceptual model of a single, large-volume magma chamber that periodically reactivates is not supported by the data. Rather, source rocks for post-caldera magmatism form from new bodies and replenish with new magmas. New basalt intrusions into the solidifying batholith are required to form the youngest volcanic rocks that erupt as independent rhyolites.

Our model of the largest Yellowstone gravity anomaly (Fig. 7) suggests a Yellowstone magma reservoir that extends 30 km northeast of the seismically imaged melt (Husen et al., 2004), compatible with Binderman et al.'s (2008) model. Hence the gravity anomaly north and northeast of the caldera may represent young fertile magma that may be more likely to erupt than melt bodies under the caldera (Fig. 8).

The distribution of silicic melt is also of interest. The local earthquake tomography of Husen et al. (2004) indicates that the partial melt body is shallowest beneath the Mallard Lake and Sour Creek

resurgent domes. The gravity modeling filtered out smaller features, but the density model suggests that partial melt is relatively shallow (10 km) over the entire length of the caldera and notably shallower (7 km) ~10 to 20 km beyond the northeastern boundary of the Yellowstone caldera. Tomographic images of Husen et al. (2004) are poorly resolved northeast of the caldera because of a lack of seismic data sources. The circular pattern of Mirror Plateau fault zone (MPFZ) faults is similar to that of the 0.6 Ma caldera, and they are thought to have acted as a ring fracture zone between the second caldera eruption at 1.2 Ma and the youngest caldera collapse 640,000 years ago (Christiansen, 2001). These faults thus predate the last caldera-forming eruption, and their presence may have favored ascension of partial melt northeast of the caldera. The density model presented here also suggests that the body of partial melt has variable density, although the gravity anomaly may also reflect changing thickness of the partial melt body or deeper thermal variations neglected here. The density is at its minimum ( $2470 \text{ kg/m}^3$ ) just beyond the northeastern border of the caldera, where it is also the shallowest (7 km). Beneath the rest of the caldera the partial melt has a density of  $2520 \text{ kg/m}^3$  and occurs at a depth of 10 km. High geothermal gradient beneath the Yellowstone caldera results in a very weak crust. Our strength models predict the brittle–ductile transition in the Yellowstone caldera to

occur at 4 km, a value independently determined by the focal depth maxima modeling in Smith et al. (2009–this volume). The models also predict that the lower crust and mantle are ductile. Temperature has the largest effect on modeled strength, and predicting the temperature at depth is difficult, but advection of mantle hotspot magmas clearly elevates crustal temperatures in the Yellowstone region.

## 6.2. The Eastern Snake River plain

The eastern SRP volcanic system represents the track of the Yellowstone hotspot to 10 million years ago (Fig. 1), reflecting modification and addition of continental crust by Yellowstone magmatic processes. Our interpreted crustal structure of the SRP shown in Fig. 6, helps clarify this transition from active hotspot to quiescent hotspot track occurs.

We suggest that basalt repeatedly ascends through established conduits, and the crust becomes depleted of low temperature melting components required for rhyolitic volcanism. Over millions of years, silicic melts solidify and allow the parental mafic magma to reach the surface, resulting in non-explosive basaltic volcanism, and a thin (1–2 km) layer of basalt on the surface. In time (on the order of ~5 Ma) the remnants of magmatic intrusions cool and solidify to form a sill-like body at the base of the upper crust.

The mid-crustal sill was first revealed by the seismic refraction velocity and density models of Sparlin et al. (1982). The evolution of this unusual mid-crustal sill is complex. Based on cyclic variations in the chemical composition of basalts from a drill core, Shervais et al. (2006) describe the mid-crustal sill as a complicated sequence of mafic lenses that are partially interconnected. The lenses are emplaced as magma ascends from the deep crust as described in the previous section. Each lens consists of a variable number of layers corresponding to each cycle of magmatism, which represent fractionation from primitive to more evolved material. The presence of more than one fractionation cycle per lens is indicative of magma recharge, necessary for generating the kind of rhyolites observed at Yellowstone.

The shape of the mid-crustal sill reflects the tendency of molten material to ascend through established conduits (Fig. 6). Thickness variations in the mid-crustal sill modeled here suggest localized concentration of magmatic ascent on scales of roughly 60 km, evocative of the regular spacing of subduction zone volcanoes. The sill is thicker in areas nearer to established conduits because these areas are easier for magmas to traverse. This is further evidenced by a decrease in the crustal component of lavas with time (Shervais et al., 2006).

The bulk composition of the mid-crustal sill suggested by Shervais et al. (2006) is approximately gabbroic. However, our velocity–density analysis implies that the bulk composition of the sill is between those of granite and gabbro. Regional seismic studies used in the analysis cannot resolve the structure of the sill into thin lenses, and thus we treat it as a homogeneous body. The inter-fingering of the gabbroic lenses and granitic upper crust could produce a bulk composition that appears intermediate on seismic records. Inter-fingering results from the repeated injection of various magma batches ponding at different levels in the crust. The density model also treats the mid-crustal sill as a large, homogeneous mass. The density of 2900 kg/m<sup>3</sup> represents an average of the mafic lenses and upper crust.

The Bouguer anomaly map (Fig. 3) shows that the SRP gravity high extends well beyond the southeastern border of the volcanic and topographic expression of the SRP. Moreover, the earthquake patterns extend further outward on the southern side of the plain than on the northern side (Fig. 5). Our model suggests that the mid-crustal sill also extends at least 10 to 20 km beyond the southeastern boundary of the SRP (Fig. 4), implying that intrusive processes at depth are not confined to the physiographic boundaries of the SRP. This geometry of the sill may also explain why in the last 5 million years, basaltic volcanism has been more voluminous to the south of the SRP than to the north,

implying that a magmatic source similar to the one beneath the SRP also exists south of the plain.

The crust in the SRP has moderate strength exceeding that of the Yellowstone caldera, but weaker than the crust in the neighboring Basin and Range province. Even though the hotspot passed beneath the SRP millions of years ago, the crust remains unusually hot (Jackson et al., 1993; Blackwell and Richards, 2004), with an approximate heat flow of 100 mW/m<sup>2</sup>. New seismic tomography of the entire plume system by Jordan et al. (2005) and summarized by Smith et al. (2009–this volume) suggests that the Yellowstone plume dips 60° to the west, in the upper mantle beneath and west of the SRP. This geometry may explain why the crustal temperatures in the SRP remain elevated despite the cessation of silicic volcanism. Upper mantle, plume derived basaltic melts may still ascend intermittently into the crust, transmitting heat and resulting in the sporadic basaltic volcanism observed today.

## 6.3. The Yellowstone to Snake River plain transition zone

The transition zone between Yellowstone and the eastern SRP roughly corresponds to the location of the second Yellowstone caldera-forming eruption, the 1.2 Ma Henry's Fork caldera, in the Island Park area, ~20 km west of Yellowstone and extending ~50 km into the basalts of the SRP. The earliest of the three Yellowstone calderas overlaps the transition zone. The transition zone straddles not only the change from the basalt-covered, seismically quiescent hotspot track to the active volcanic system, but also the transition from extended Basin and Range lithosphere toward more stable and much older basement of the Wyoming craton. A lack of seismic and geodetic data has hindered modeling of this area, and this study provides the first interpretation of the density structure.

The presence of the mid-crustal sill in the SRP and the partial melt in Yellowstone imply that YSRP volcanism is a continuous process. The steady decrease in the gravity from the +40 Mgal high in the eastern SRP to the –50 Mgal low in Yellowstone suggests a mid-crustal density greater than that of the partial melt in Yellowstone and less than that of the mid-crustal sill in the SRP, implying a “transitional sill” between dense SRP intrusions and the Yellowstone partial melt. A density of 2820 kg/m<sup>3</sup> was estimated by increasing the density by increments of 100 kg/m<sup>3</sup> from the partial melt density of 2520 kg/m<sup>3</sup> in the southeastern part of Yellowstone while keeping the size and shape of the body generally consistent with the size and shape of the sill and the partial melt. The location of the change between the mid-crustal sill in the SRP and the “transitional sill” in the YSRP transition zone is somewhat arbitrary. The transitional sill can extend ~10–20 km deep farther west beneath the SRP if it is 2 to 3 km thicker, or farther east if it is thinner. Using a linear velocity–density relationship from the velocity–density estimates derived in Section 4 (excluding the mafic and Yellowstone partial melts), the P-wave velocity of the transitional sill is ~6.35 km/s, between those of the mid-crustal sill (6.5 km/s) and the Yellowstone partial melt (4.6 km/s). This body is interpreted to be structurally similar to the mid-crustal sill, but has not yet completely cooled and solid.

While there are basalt flows in Yellowstone and the Island Park area, widespread basaltic volcanism like that observed in the eastern SRP has not yet occurred in the transition zone southwest of the Yellowstone caldera. Christiansen (2001) explains this lack of basalt by suggesting that the subsurface magma chamber has not cooled enough to develop cracks to permit passage of basalt from below. This is a reasonable hypothesis, but it is difficult to address with the data and methodology in this study. The gravity measurements suggest that the sill and overlying silicic rocks in this region have not cooled and densified sufficiently to lend positive buoyancy to intruding basalt magmas.

## 7. Concluding remarks

A combination of gravity, seismic, thermal, rheological, and petrologic data was used to model the density, rheological structure and composition of the YSRP volcanic system. Seismic velocity models were used to constrain the three-dimensional density structure with the aid of velocity–density relations based on petrologic information. Strength profiles were modeled at several locations and compared to

accurate earthquake focal depths. This information aids the interpretation of the tectonic and magmatic processes that have shaped the region.

A summary cross section of the resulting composition and density–velocity structure of the YSRP volcanic field is shown in Fig. 12. The hotspot processes that produce observed YSRP features are complex and varied. Basaltic material at mantle hotspot temperatures (~1500 °C) rises from the mantle into the lower crust. Clinopyroxene

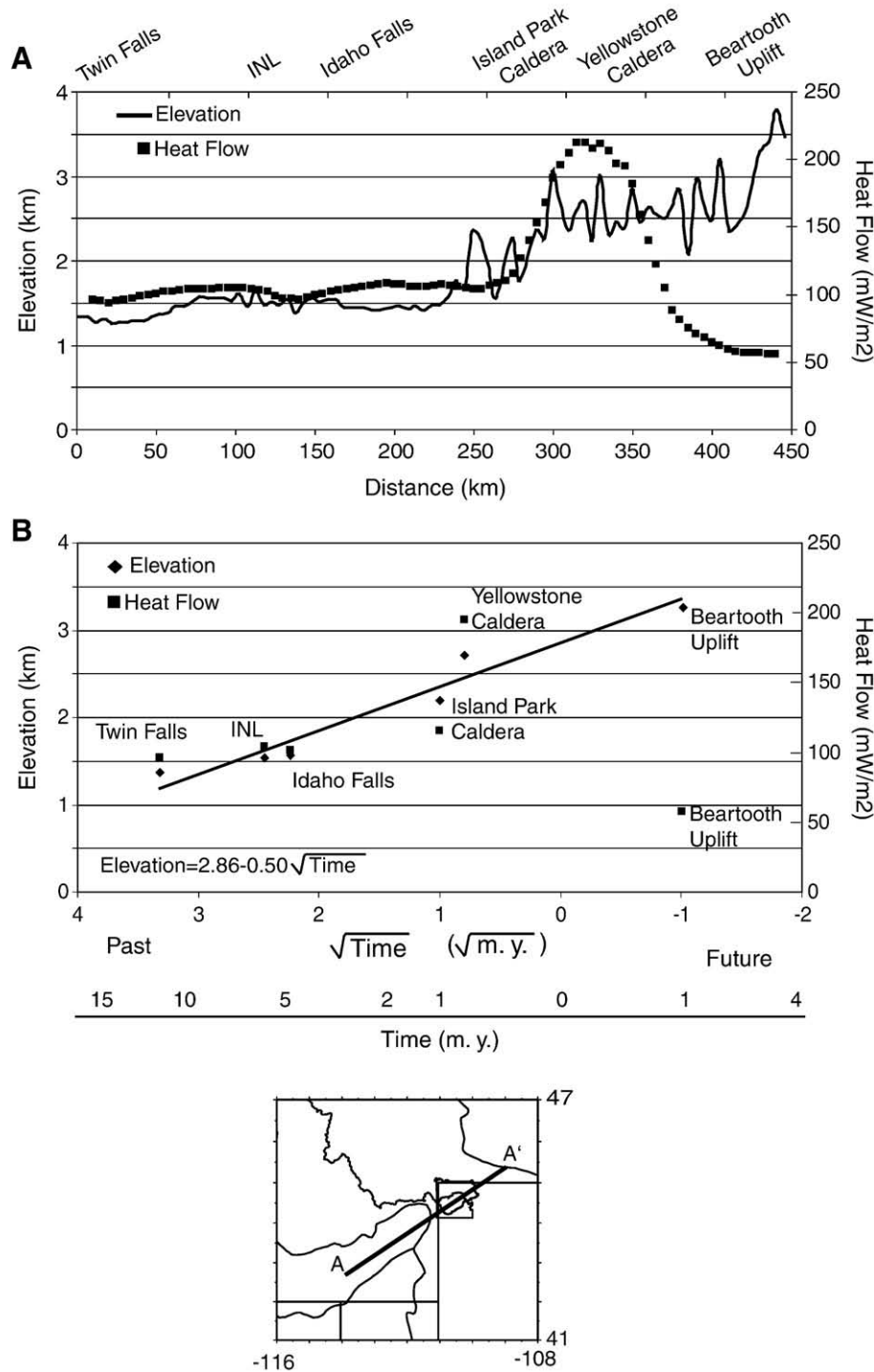


**Fig. 13.** Generalized relationships between elevation (km), heat flow (mW/m<sup>2</sup>), and volcanic age along the track of the Yellowstone hotspot. A. Plots of elevation (km) and surface heat flow from Blackwell and Richards (2004). Heat flow and elevation increase with increasing distance along the hotspot track. B. A plot of elevation and heat flow vs. the square root of time (where time is the age of silicic volcanic rocks in millions of years from Armstrong et al. (1975)) shows an approximately linear decay of elevation with the square root of time comparable to the lithospheric cooling described by Smith and Braile (1993).

fractionation at the Moho (~40 km) forms an underplated layer at the base of the crust with density 3200 kg/m<sup>3</sup> and P-wave velocity 7.25 km/s. The resulting, more buoyant mafic melt then ascends to the crust, feeding a mixed body of silicic and basaltic partial melt. In this active volcanic system, there is enough felsic material to produce a cap of rhyolitic melt that escapes during caldera forming eruptions. The gravity modeling suggests that the silicic melt has a density of 2470 to 2520 kg/m<sup>3</sup>, with the lowest density, shallowest (7 km) material occurring beyond the northeastern edge of the caldera.

Our models suggest that magma preferentially ascends through thermally processed conduits, and in time these conduits become depleted of low temperature melting materials required for rhyolitic volcanism. Repeated injection of basalt results in a sequence of mafic lenses in the upper crust. As the North American Plate passes over the hotspot and the heat source is removed, any remaining silicic melt solidifies. At this temperature and stress state it becomes possible for basaltic melt to reach the surface. As the plate moves further from the heat source, the basaltic melts also solidify, resulting in a mid-crustal sill. The density and velocity of the sill are 2900 kg/m<sup>3</sup> and 6.5 km/s, respectively.

These properties suggest that the bulk composition of the mid-crustal sill is dioritic, although the bulk properties probably represent averaging of mafic lenses inter-fingered with the granitic upper crust. In the transition between the SRP characterized by its ubiquitous mid-

crustal mafic sill and effusive basalt cover, and the Yellowstone caldera with its mid- to upper-crustal magma chamber, the upper crust consists of a cooling, crystallizing sill inferred to represent the stage during which silicic melts solidify. The lack of positive buoyancy for basalt magmas intruding this body would account for a lack of widespread basaltic volcanism in the Island Park area. The velocity–density analysis suggests that the transitional sill has a density of 2820 kg/m<sup>3</sup> and a P-wave velocity of 6.35 km/s, intermediate between Yellowstone and the eastern SRP.

A key finding of our study is the recognition that the Yellowstone magma system extends up to 20 km northeast of the mapped caldera boundary, where it is 3 km shallower than beneath the Sour Creek resurgent dome. This result suggests that if new melt is required for continued Yellowstone volcanism (e.g., Bindeman et al., 2008) then the crust northeast of the mapped caldera may be more susceptible to volcanism than the rest of the caldera. Also we find that the mid-crustal sill observed along the length of the eastern SRP extends laterally southeast ~20 km beyond the physiographic province boundary. This asymmetry is also noted in the seismicity and youthfulness of faulting extending into southeastern Idaho.

Strength modeling of the YSRP system reveals that temperature has the greatest influence on strength in the YSRP (Fig. 11). Fig. 13 illustrates the relationship between elevation, heat flow, distance along the hotspot track, and time. Both elevation and heat flow

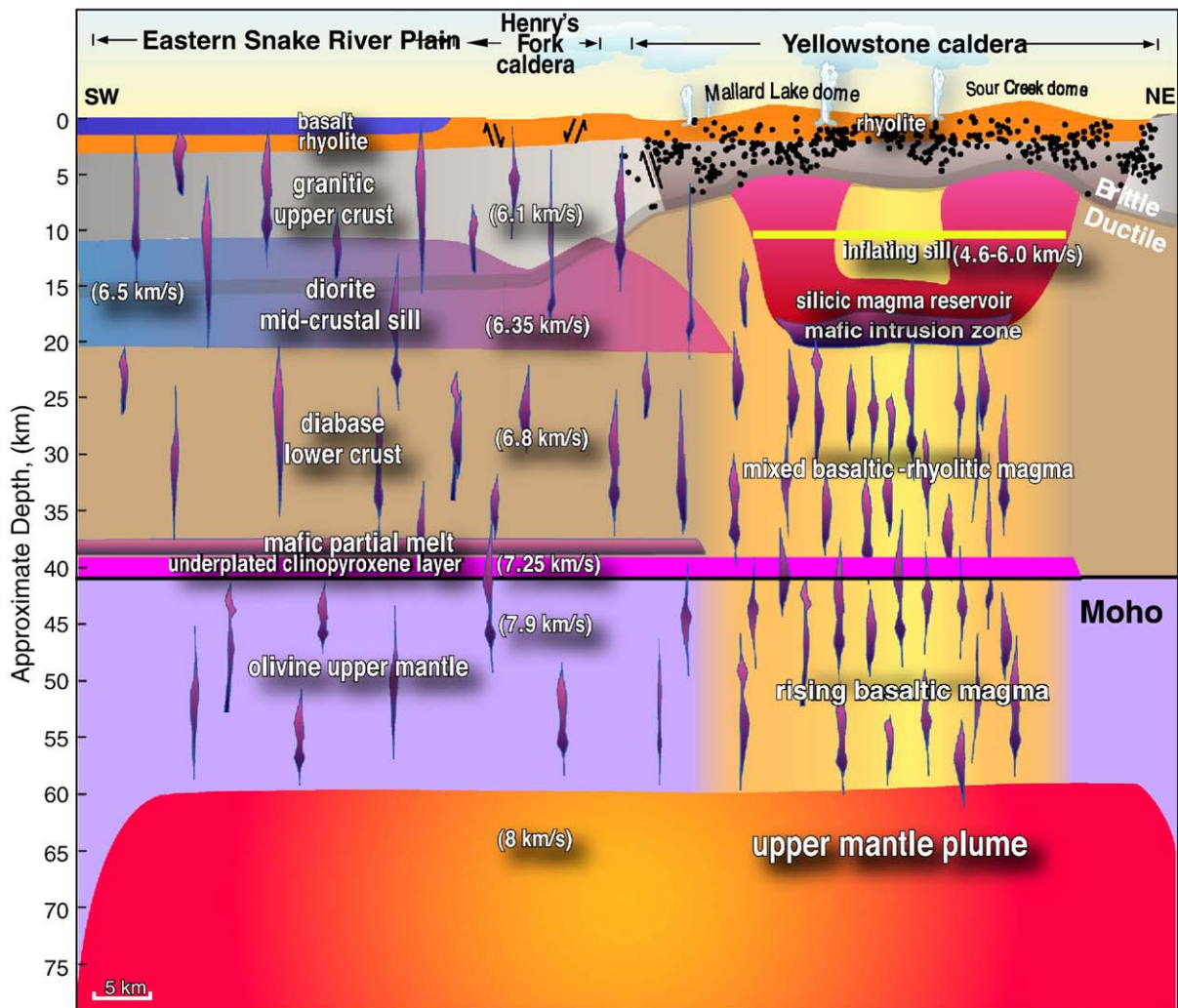


Fig. 14. Cross section of the YSRP summarizing the model of crustal structure, composition and magmatic processes interpreted from this and other studies.

systematically increase with decreasing distance from Yellowstone. This relationship implies that variations in elevation of the YSRP are primarily related to thermal mechanisms.

The new gravity data and constrained modeling presented here provide an integrated model of the Yellowstone hotspot magmatic processes that have highly modified the continental lithosphere (Fig. 14). Importantly it provides a model of magmatic evolution from the active silicic volcanism at Yellowstone to the well-evolved basalt–rhyolite volcanism of the SRP. Unresolved topics of the YSRP evolution include the enigmatic seismic quiescence of the SRP. Strain rates of the surrounding seismically active areas of active Basin–Range normal faulting are high, but it remains unclear whether the SRP behaves differently because the high density mid-crustal sill imparts strength to the lithosphere, or because high temperatures affect the seismogenic capability, or deformation is limited to volcanic episodes.

## Acknowledgements

We appreciate the thoughtful comments and discussions of our project with Barbara Nash, John Shervais, Rick Blakely, Jonathan Glen, David Hill and Michael Jordan. The gravity data were compiled from multiple surveys in the study area and are from an online archive at the Pan American Center for Earth and Environmental Studies. Randy Keller was very helpful in matters of downloading and interpreting gravity and magnetic data from the PACES archive.

David Blackwell and Maria Richards of Southern Methodist University were very helpful in providing and interpreting unpublished heat flow and temperature data of the YSRP. Suzette Jackson Payne of the Idaho National Laboratory (INL) provided earthquake information from the eastern SRP area. Yellowstone and surrounding area earthquake data were from the archives of the Yellowstone seismic network recorded at the University of Utah Seismograph Stations and the Montana Bureau of Mines and Geology seismic network. Christine Puskas and Jamie Farrell assisted with illustration preparation. Funding was provided by the NSF funded GEOsciences Network (GEON) project, EAR-0724265.

## References

- Anders, M.H., Sleep, N.H., 1992. Magmatism and extension: the thermal and mechanical effects of the Yellowstone hotspot. *J. Geophys. Res.* 97, 15379–15393.
- Armstrong, R.L., Leeman, W.P., Malde, H.E., 1975. K–Ar dating, Quaternary and Neogene volcanic rocks of the Snake River Plain, Idaho. *Am. J. Sci.* 275 (3), 225–251.
- Asimow, P.D., Ghiorso, M.S., 1998. Algorithmic modifications extending MELTS to calculate subsolidus phase relations. *Am. Mineral.* 83, 1127–1131.
- Bindeman, N., Fu, B., Kita, N.T., Valley, J.W., 2008. Origin and evolution of Yellowstone silicic magmatism based on ion microprobe analysis of isotopically-zoned zircons. *J. Pet.* 49, 163–193.
- Blackwell, D.D., Richards, M.C., 2004. Geothermal Map of North America. American Association of Petroleum Geologists, 1 sheet, scale 1:6,500,000.
- Blackwell, D.D., Negraru, P.T., Richards, M.C., 2007. Assessment of the enhanced geothermal system resource base of the United States. *Nat. Resour. Res.* 15 (4), 283–308. doi:10.1007/s11053-007-9028-7.
- Blakely, R.J., 1996. *Potential Theory in Gravity and Magnetic Applications*. Cambridge University Press, Cambridge, UK, 464 pp.
- Bonnichsen, B., 1982. Rhyolite lava flows in the Bruneau–Jarbridge Eruptive Center, Southwestern Idaho. In: Bonnichsen, B., Breckenridge, R.M. (Eds.), *Cenozoic Geology of Idaho*, vol. 26. Idaho Bureau of Mines and Geology Bulletin, Moscow, ID, pp. 283–320.
- Braile, L.W., Smith, R.B., Anson, J., Baker, M.R., Sparlin, M.A., Prodehl, C., Schilly, M.M., Healy, J.H., Mueller, S., Olsen, K., 1982. The Yellowstone Snake River Plain seismic profiling experiment: crustal structure of the eastern Snake River Plain. *J. Geophys. Res.* 84, 2597–2610.
- Brott, C.A., Blackwell, D.D., Ziegler, J.P., 1981. Thermal and tectonic implications of heat flow in the eastern Snake River Plain. *J. Geophys. Res.* 86, 11709–11734.
- Camp, V.E., Ross, M.E., 2004. Mantle dynamics and genesis of mafic magmatism in the intermontane Pacific Northwest. *J. Geophys. Res.* 109, B08204. doi:10.1029/2003JB002838.
- Carle, S.F., Glen, J.M., Langenheim, E., Smith, R.B., Oliver, H.W., 1990. Isostatic gravity map and principal facts for 694 gravity stations in Yellowstone National Park and vicinity, Wyoming, Idaho, and Montana. U. S. Geological Survey Open-File-Report 90-694. U. S. Geol. Surv., Denver, CO. 34 pp.
- Chapman, D.S., 1986. Thermal state of the continental lower crust. In: Dawson, J., Carswell, D., Hall, J., Wedepohl, K. (Eds.), *The Nature of the Lower Continental Crust*. Geol. Soc. Spec. Pub., London, pp. 63–70.
- Christiansen, R.L., 1984. Yellowstone magmatic evolution: its bearing on understanding large-volume explosive volcanism. *Explosive Volcanism: Its Inception, Evolution, and Hazards*. National Research Council Studies in Geophysics. National Academy Press, Washington, D.C., pp. 84–95.
- Christiansen, R.L., 2001. The Quaternary and Pliocene Yellowstone Plateau volcanic field of Wyoming, Idaho, and Montana. U. S. Geological Survey Professional Paper 729-G. U. S. Geol. Surv., Denver, CO. 146 pp.
- Christiansen, R.L., Blank, H.R., 1969. Volcanic evolution of the Yellowstone rhyolite plateau and eastern Snake River Plain. Symposium on Volcanoes and Their Roots. Int. Assoc. Volc. Chem. Earth's Interior, Oxford, pp. 220–221.
- Christiansen, R.L., Foulger, G.R., Evans, J.R., 2002. Upper-mantle origin of the Yellowstone Hotspot. *Geol. Soc. Am. Bull.* 114 (10), 1245–1256.
- Crisp, J.A., 1984. Rates of magma emplacement and volcanic output. *J. Volcanol. Geotherm. Res.* 20, 177–211.
- Fujii, T., Kushiro, I., 1977. Density, viscosity and compressibility of basaltic liquid at high pressures. Year Book Carnegie Inst. Washington, vol. 76, pp. 419–424.
- Ghiorso, M.S., Hirschmann, M.M., Reiners, P.W., Kress, V.C., 2002. The pMELTS: a revision of MELTS aimed at improving calculation of phase relations and major element partitioning involved in partial melting of the mantle at pressures up to 3 GPa. *Geochem. Geophys. Geosyst.* 3 (5). doi:10.1029/2001GC000217.
- Hacker, B.R., Abers, G.A., 2004. Subduction Factory 3: an Excel worksheet and macro for calculating the densities, seismic wave speeds, and H<sub>2</sub>O contents of minerals and rocks at pressure and temperature. *Geochem. Geophys. Geosyst.* 5 (1). doi:10.1029/2003GC000614.
- Hildreth, W., Halliday, A.N., Christiansen, R.L., 1991. Isotopic and chemical evidence concerning the genesis and contamination of basaltic and rhyolitic magma beneath the Yellowstone Plateau volcanic field. *J. Pet.* 32, 63–138.
- Humphreys, E.D., Dueker, K.G., Schutt, D.L., Smith, R.B., 2000. Beneath Yellowstone: evaluating plume and nonplume models using teleseismic images of the upper mantle. *GSA Today* 10 (12), 1–7.
- Husen, S., Smith, R.B., Waite, G.P., 2004. Evidence for gas and magmatic sources beneath the Yellowstone volcanic field from seismic tomographic imaging. *J. Volcanol. Geotherm. Res.* 131, 397–410.
- Jackson, S.M., Wong, I.G., Carpenter, G.S., Anderson, D.M., Martin, S.M., 1993. Contemporary seismicity in the eastern Snake River Plain, Idaho, based on microearthquake monitoring. *Seismol. Soc. Am. Bull.* 83, 680–695.
- Jordan, M., Smith, R.B., Puskas, C.M., Farrell, J., Waite, G.P., 2005. The Yellowstone hotspot and related plume: volcano-tectonics, tomography, kinematics, dynamics, and mantle flow. *Eos Trans. AGU* 86 (52) Fall Meet. Suppl., Abstract T51D-1388.
- Krukoski, J.C., 2002. A geologic database (GeoGIS) and three-dimensional inversion for the density structure of the Yellowstone volcanic system. M.S. Thesis, University of Utah, Salt Lake City, UT, 96pp.
- Leeman, W.P., 1982. Development of the Snake River Plain–Yellowstone Plateau Province, Idaho and Wyoming: an overview and petrologic model. In: Bonnichsen, B., Breckenridge, R.M. (Eds.), *Cenozoic Geology of Idaho*, vol. 26. Idaho Bureau of Mines and Geology Bulletin, Moscow, ID, pp. 155–177.
- Leeman, W.P., Menzies, M.A., Matty, D.J., Embree, G.F., 1985. Strontium, neodymium, and lead isotopic compositions of deep crustal xenoliths from the Snake River Plain: evidence for Archean basement. *Earth Planet. Sci. Lett.* 75, 354–368.
- Lehman, J.A., Smith, R.B., Schilly, M.M., Braile, L.W., 1982. Upper crustal structure of the Yellowstone caldera from delay time analyses and gravity correlations. *J. Geophys. Res.* 87 (B4), 2713–2730.
- Lowenstern, J.B., Hurwitz, S., 2008. Monitoring a supervolcano in repose: heat and volatile flux at the Yellowstone Caldera. *Elements* 4 (1), 35–40.
- Lowry, A.R., Ribe, N.L., Smith, R.B., 2000. Dynamic elevation of the Cordillera, Western United States. *J. Geophys. Res.* 105 (10), 23371–23390.
- Lum, C.C.L., Leeman, W.P., Foland, K.A., Kargel, J.A., Fitton, J.G., 1989. Isotopic variations in continental basaltic lavas as indicators of mantle heterogeneity: examples from the Western U. S. Cordillera. *J. Geophys. Res.* 94, 7871–7884.
- Lynch, D.P., 1998. Three-dimensional finite difference tomography of the Basin and Range–Colorado Plateau–Rocky Mountain transition using earthquake and controlled source data. M.S. Thesis, University of Utah, Salt Lake City, Utah, 155 pp.
- Lynch, D., Smith, R.B., Benz, H.M., 1997. Three-dimensional tomographic inversion of crust and upper mantle structure of the eastern Basin Range–Rocky Mountain transition from earthquake and regional refraction data. Abstracts from the 9th Annual IRIS Workshop, the IRIS Consortium, Breckenridge, Colorado, June 8–12, 1997.
- Mabey, D.R., Peterson, D.L., Wilson, C.W., 1974. Preliminary gravity map of southern Idaho. U. S. Geological Survey Open-File-Report. U. S. Geol. Surv., Reston, VA, pp. 74–78. 1 pp.
- McQuarrie, N., Rodgers, D.W., 1998. Subsidence of a volcanic basin by flexure and lower crustal flow: the eastern Snake River Plain, Idaho. *Tectonics* 17, 203–220.
- Morgan, P., Blackwell, D.D., Spafford, R.E., Smith, R.B., 1977. Heat flow measurements in Yellowstone Lake and thermal structure of the Yellowstone caldera. *J. Geophys. Res.* 82, 3719–3783.
- Nash, B.P., Perkins, M.E., Christensen, J.N., Lee, D., Halliday, A.N., 2006. The Yellowstone hotspot in space and time: Nd and Hf isotopes in silicic magmas. *Earth Planet. Sci. Lett.* 247, 143–156.
- Parsons, T., Thompson, G.A., Smith, R.P., 1998. More than one way to stretch: a tectonic model for extension along the plume track of the Yellowstone hotspot and adjacent Basin and Range Province. *Tectonics* 17, 221–234.
- Payne, S.J., McCaffrey, R., King, R.W., 2008. Strain rates and contemporary deformation in the Snake River Plain and surrounding Basin and Range from GPS and seismicity. *Geology* 36 (8), 647–650. doi:10.1130/G25309A.1.
- Peng, X., Humphreys, E.D., 1998. Crustal velocity structure across the eastern Snake River Plain and the Yellowstone swell. *J. Geophys. Res.* 103, 7171–7186.
- Perkins, M.E., Nash, B.P., 2002. Explosive silicic volcanism of the Yellowstone hotspot: the ash fall tuff record. *Geol. Soc. Am. Bull.* 114 (3), 367–381.

- Pierce, K.L., Morgan, L.A., 1992. The track of the Yellowstone hot spot: volcanism, faulting, and uplift. In: Link, P.K., Kuntz, M.A., Platt, L.B. (Eds.), *Regional Geology of Eastern Idaho and Western Wyoming*. In: Geological Society of America Memoir, vol. 179. Geological Society of America, Boulder, CO, pp. 1–53.
- Puskas, C.M., Smith, R.B., 2009. Intraplate deformation and microplate tectonics of the Yellowstone hotspot and surrounding Western U.S. interior. *J. Geophys. Res.* 114, B04410. doi:10.1029/2008JB005940.
- Puskas, C.M., Smith, R.B., Meertens, C.M., Chang, W.L., 2007. Crustal deformation of the Yellowstone–Snake River Plain volcano-tectonic system: campaign and continuous GPS observations, 1987–2004. *J. Geophys. Res.* 112. doi:10.1029/2006JB004325.
- Raymond, L.A., 2002. *The Study of Igneous, Sedimentary, and Metamorphic Rocks*. McGraw-Hill, New York, NY, 736 pp.
- Schilly, M.M., Smith, R.B., Braile, L.W., Ansorge, J., 1982. 1978 Yellowstone–eastern Snake River Plain seismic profiling experiment: data and upper crustal structure of the Yellowstone region. *J. Geophys. Res.* 87, 2692–2704.
- Schmidt, S., Gotze, H.J., 1998. Interactive visualization and modification of 3D models using GIS functions. *Phys. Chem. Earth* 23, 289–295.
- Shervais, J.W., Vetter, S.K., Hanan, B.B., 2006. Layered mafic sill complex beneath the eastern Snake River Plain: evidence from cyclic geochemical variations in basalt. *Geology* 34, 365–368.
- Smith, R.B., Bruhn, R.L., 1984. Intraplate extensional tectonics of the Western U.S. Cordillera: inferences on structural style from seismic reflection data, regional tectonics and thermal–mechanical models of brittle–ductile deformation. *J. Geophys. Res.* 89 (B7), 5733–5762.
- Smith, R.B., Braile, L.W., 1993. Topographic signature, space–time evolution, and physical properties of the Yellowstone–Snake River Plain volcanic system: the Yellowstone hotspot. In: Snoko, A.W., Steidtmann, J.R., Roberts, S.M. (Eds.), *Geology of Wyoming: Geological Survey of Wyoming Memoir No. 5*. American Geophysical Union, Washington, D.C., pp. 694–754.
- Smith, R.B., Siegel, L.J., 2000. *Windows Into The Earth, The Geologic Story of Yellowstone and Grand Teton National Parks*. Oxford University Press, New York, 242 pp.
- Smith, R.B., Braile, L.W., Schilly, M., Ansorge, J., Prodehl, C., Baker, M., Healey, M., Mueller, H.S., Greensfelder, R., 1982. The Yellowstone–eastern Snake River Plain seismic profiling experiment: crustal structure of Yellowstone. *J. Geophys. Res.* 84, 2583–2596.
- Smith, R.B., Jordan, M., Steinberger, R., Puskas, C.M., Farrell, J., Waite, G.P., Husen, S., Chang, W.-L., O'Connell, R., 2009. Geodynamics of the Yellowstone hotspot and mantle plume: seismic and GPS imaging, kinematics, and mantle flow. *J. Vol. Geotherm. Res.* 188, 26–56.
- Sparlin, M.A., Braile, L.W., Smith, R.B., 1982. Crustal structure of the eastern Snake River Plain determined from ray trace modeling of seismic refraction data. *J. Geophys. Res.* 87, 2619–2633.
- Stachnik, J.C., Dueker, K., Schutt, D.L., Yuan, H., 2008. Imaging Yellowstone plume–lithosphere interactions from inversion of ballistic and diffusive Rayleigh wave dispersion and crustal thickness data. *Geochem. Geophys. Geosyst.* 9, Q06004. doi:10.1029/2008GC001992.
- White, B.J.P., Smith, R.B., Husen, S., Farrell, J.M., Wong, I., 2009. Seismicity and earthquake hazard analysis of the Teton–Yellowstone region, Wyoming. *J. Vol. Geotherm. Res.* 188, 277–296.